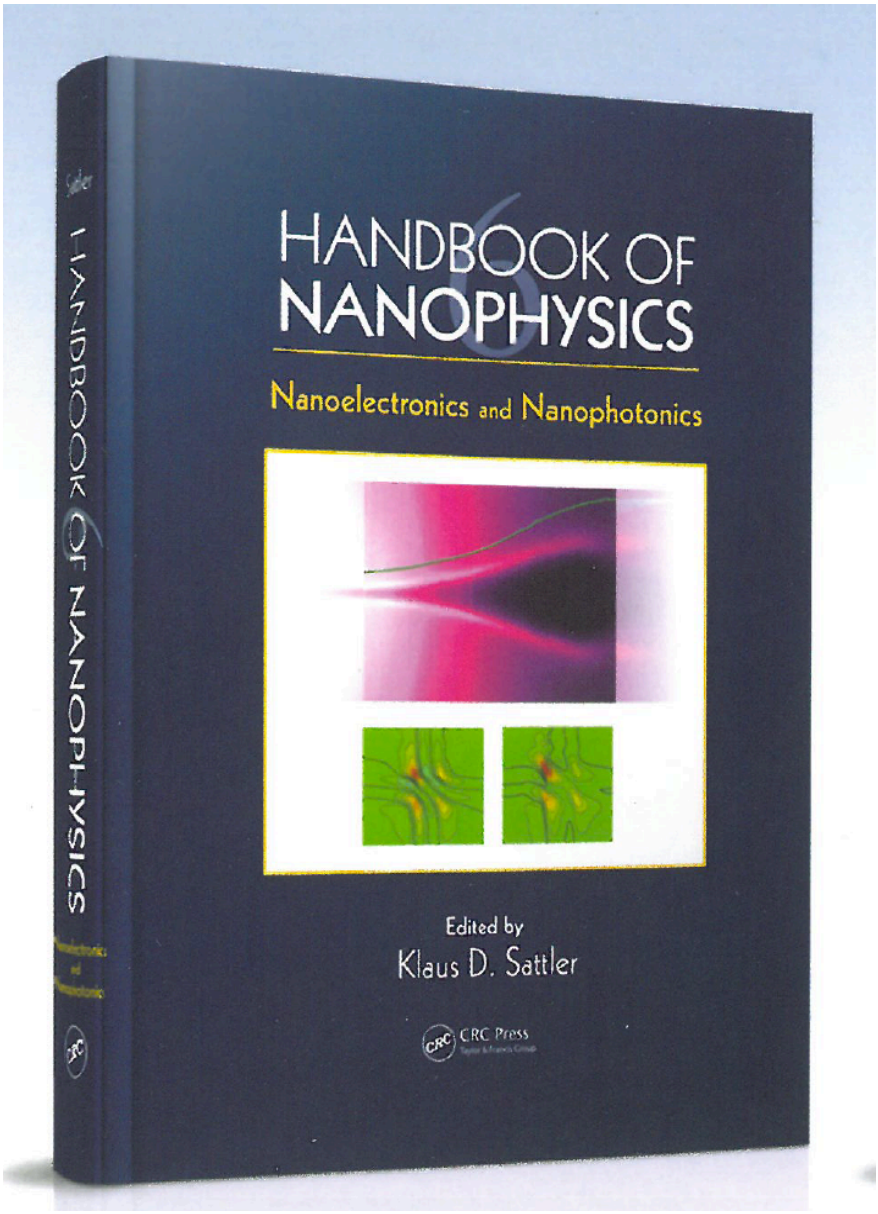

Volume 6: Nanoelectronics and Nanophotonics

Computing and Nanoelectronic Devices. Nanoscale Transistors. Nanolithography. Optics of Nanomaterials. Nanophotonic Devices. Nanoscale Lasers. Index.

Catalog no. 75500, September 2010, 784 pp., ISBN: 978-1-4200-7550-2, $139.95 / £89.00

7

Superconducting Weak Links Made of Carbon Nanostructures

Vincent Bouchiat
Centre National de la Recherche Scientifique

7.1 Introduction

It has been known since the 1960s (De Gennes and Guyon 1963) that charge carriers emitted from a superconductor can propagate in a non-superconducting medium, provided that the electron wave functions of the two electrons originating from the superconductor (the so-called Cooper pairs) keep their correlation during their diffusion outside the superconductor. This process requires the absence of defects in the propagating medium that break time-reversal symmetry, such as magnetic impurities. These correlated electrons form an evanescent state that "bleeds" from the superconductors into the non-superconducting electrode on mesoscopic distances. The physics of these evanescent states, known as the "superconducting proximity effect" depends on many parameters (the coherence length of the superconductor, the contact barrier at the interface, the temperature, the electron diffusion length, etc.).

It appeared then possible to sever a superconducting electrode with non-superconducting elements (a narrow constriction, a normal metal, a thin insulating barrier, known as "weak links") while keeping a supercurrent flow. As tunneling processes are known to depend exponentially on the thickness of oxide barriers, controlling the structure and the geometry of weak links down to the atomic scale appears to be of capital importance if one wants to get reproducible devices. Therefore, improving the miniaturization and the crystalline quality of these weak links was clearly identified as a critical issue. Among the possible candidates are sp^2-hybridized carbon nanostructures (i.e., graphenes, carbon nanotubes [CNTs], or fullerenes), which, among other advantages, offer good control of the crystallinity and provide ideal media to control a supercurrent flow. Quantum confinement of electronic states within the carbon nanostructure generates sharp variations of the electronic density of states. Tuning the weak link chemical potential with an electrostatic gate allow to adjust the weak link transparency.

The purpose of this chapter is to propose a basic overview of the principles that govern the physics of these carbon based

devices and illustrate them by presenting experimental demonstrations and some applications.

7.2 Superconducting Transport through a Weak Link

7.2.1 Density of Electronic States in a Superconductor

At energies around the chemical potential μ and below the energy gap Δ, a superconductor (noted in the following by the symbol S) only has a single ground state, which depends on a macroscopic phase. In a bulk superconductor, all electrons are in the same quantum state characterized by a global phase φ. The charge carriers are condensed in a bound state of two electrons, the so-called Cooper pair, which has a charge of $-2e$ (Figure 7.1a). The ground state wave function depends on the phase φ and can be written as

$$\Delta \approx \sqrt{n_s}\exp(i\varphi), \tag{7.1}$$

where n_s is the total number of Cooper pairs.

Δ is the "superconductor order parameter" and specifies the choice for the quantum phase φ. There are no other states present in the interval $[\mu - \Delta, \mu + \Delta]$ because it takes an energy 2Δ to break a Cooper pair. An electron in this energy window cannot be injected in a superconductor alone, generating a "gap" in the transmission of charge carriers at a normal/superconductor metal interface.

7.2.2 Coherent Transport at a Normal/Superconducting Interface

At the interface between a normal metal (N) and a superconductor (S), an electron at the Fermi level can nevertheless be converted into a Cooper pair with zero momentum if a hole (charge + *e*) is reflected with energy −ε and opposite momentum, conserving the charge, energy, and momentum. The reflected hole acquires an additional phase factor φ, the order parameter phase. This conversion of an electron–hole pair into a Cooper pair is a process known as the Andreev reflection (Figure 7.1b). It dominates the charge transport at low bias through the interface. This Andreev reflection can lead to a supercurrent transport if correlated charge carriers are collected by a second superconductor placed in a series. The process is still effective at the interface between superconducting electrodes and nanoscale constriction, which we will refer to as a "weak link."

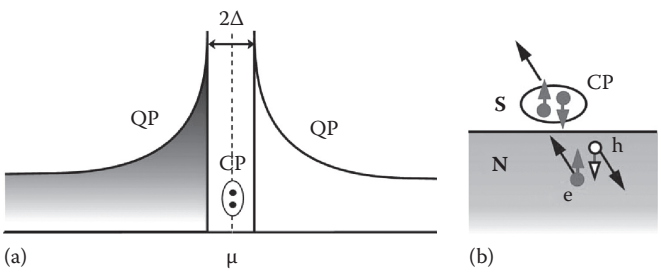

FIGURE 7.1 (a) Density of state of a superconducting electrode: all the electrons are in the ground state wave function at the chemical potential μ. (b) Schematics depicting the Andreev reflection. Describing coherent transport at a normal/superconducting interface below the gap. An electron (e) impinging the interface between a normal conductor (N) and a superconductor (S) produces a Cooper pair (CP, oval) in the top superconducting electrode and a retro-reflected hole (h) in the normal conductor. Vertical arrows indicate the spin band occupied by each particle.

7.2.3 A Short Introduction to the Josephson Effect

The order parameter characterizing the superconducting state varies on a spatial scale equal to $\xi = h v_F/\Delta$, where v_F is the Fermi velocity. The quantity ξ, which is a measure of the size of Cooper pairs, is called the coherence length. At the interface with an insulator, a metal, or a nano-object, the superconducting order parameter $\Delta(\mathbf{r})$ (its wave function) weakens gradually close to the interface on a characteristic scale, which is on the order of ξ.

When two superconductors with phase φ_1 and φ_2 are separated by a weak link (see Figure 7.2), they interact through direct tunneling or by the Andreev reflection process presented in the previous paragraph. This sandwich structure is called a Josephson junction. It is dominated by the interaction energy between the two superconductors. In 1962, Brian Josephson predicted that due to the interaction between the two superconducting condensates in close proximity, a non-superconducting nanostructure can let flow a superconducting current *I*, the value of which depends on the phase twist between the two condensates (Figure 7.2) (Josephson 1962). For a thin insulating tunnel barrier, he has shown that the current has the following form:

$$I = I_c \sin(\varphi_2 - \varphi_1). \tag{7.2}$$

This surprising prediction (Josephson 1962) was rapidly experimentally confirmed, leading to a new field in superconducting electronics. Until the mid-1990s, such superconducting "weak links" were either made of insulating barriers (the so-called Josephson tunnel junctions, at the origin of all the recent advances in superconducting Qubits), narrow diffusive metallic

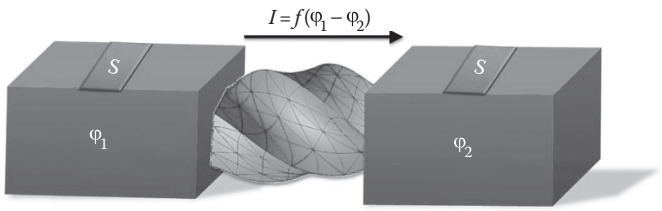

FIGURE 7.2 Schematics of a Josephson weak link. In this device, two superconducting electrodes, characterized by their phase φ_1 and φ_2 are separated by a weak link (symbolized by a twisted solid). The superconducting current *I* flowing through the weak link is a given function *f* of the "phase twist" i.e., the phase difference $\varphi_1 - \varphi_2$. This current–phase function *f* exhibits a 2π-periodicity and is highly non linear. It is the main characteristics of a Josephson weak link.

or semiconducting wires, or point contacts inserted between bulk electrodes (Likharev 1979). The first realization of a ballistic weak link with a limited number of conduction channels and controlled at the atomic scale came in 1997, with the measurement transport through gold atomic contacts in close vicinity of superconducting aluminum contacts (Scheer et al. 1997). In the last 5 years, it has been shown that carbon nanostructures can provide another class of weak links of good structural quality, for which strong quantum confinement offers gate tunability.

7.2.4 Normal Electron Transport through an Atomic or Molecular Conductor

At the atomic level, electron transport occurs by hopping through the atomic or molecular orbitals that are quantized in the case of a laterally confined nanostructure. They provide discrete conducting channels for electron transport (Imry and Landauer 1999). At the interface with a nanostructure, these contributions are related to the overlaps between molecular orbitals and the electronic wave functions in the metal. The physics of this quantum transport follows the description of Rolf Landauer from the 1970s, which refers to treating incoming charge carriers as plane waves traveling through "conduction channels" that are the eigen-modes for electronic propagation within the nanostructure. The electronic wave is partially transmitted and reflected at the interface. The theoretical work by Landauer and subsequently confirmed by numerous experiments have shown that the conductance of an electronic mesoscopic conductor is indeed divided into a discrete sum over all conduction channels i placed in parallel:

$$G = \sum_i G_i = \sum_i G_0 T_i = \frac{2e^2}{h} \sum_i T_i. \tag{7.3}$$

Each channel bears a quantized conductance G_0 called the quantum of conductance given by a ratio of two fundamental constants, $G_0 = 2e^2/h = (12.8\,\mathrm{k\Omega})^{-1}$. In practice, each conduction channel is partially coupled to the modes of the reservoirs. This induces a reduction of the conductance of a dimension-less prefactor T_i with $0 < T_i < 1$. The origin of these reduction factors is essentially of technologic origin and can be optimized by choosing the right interface materials as shown below. Nevertheless, even for a perfectly transmitting interface ($T = 1$), the normal transport through a nanoscale conductor is limited to a resistive transport of 12 kΩ per channel, the resistance being localized at the interface between the reservoir and the leads (see Figure 7.8a for an example).

In the case of coupling to superconducting electrodes, the Landauer formula 7.3 is no more valid: it is possible to cancel this contact resistance and obtain a zero-resistance electron flow through an atomic-sized contacts. This simple observation might have important technical consequences in the future of nanoelectronics, for example, to limit heat dissipation in the case of the ultra-high density integration of nanodevices involving few conduction channels.

7.2.5 Superconducting Transport through Andreev Bound States

As shown in Section 7.2.2, the microscopic transfer of charges at a superconducting interface arises by an electron–hole process known as the Andreev reflection. In a weak link, there are two normal/superconducting interfaces back-to-back (S/weak link and weak link/S). The two proximity effects on each side percolate and give rise to a superconducting current flow through the weak link. Furthermore, one has to consider the confinement in the weak link of the electron and holes created by the successive Andreev reflections at the interfaces: the electron and the holes remain spatially and energetically confined (Figure 7.3), thus defining a quantum well. The eigenstates of this well, the so-called Andreev bound states, require constructive interferences to propagate. The electron state, once converted into its hole conjugate, is converted back into the same electron state with the same quantum phase. This defines a quantization condition that depends on the phase difference between the superconductors: they shift the electron–hole Andreev wave function by their phase $\exp(i\varphi)$.

When no scattering occurs between the superconductors, there are two bound states per conductance channel with the energies $E_\pm = \pm\Delta\cos(\phi/2)$. More realistically, in the presence of a finite transmission T_i, their energies become $E_\pm = \pm\Delta\sqrt{1-\sin^2(\phi/2)}$ (Goffman et al. 2000). At low temperatures, only the Andreev-bound state lowest in energy is occupied. The Josephson superconducting currents carried by the different channels add their contribution to each other and for the superconducting current give

$$I = -\frac{\partial \sum_i E_-(\phi, T_i)}{\partial\phi} = \frac{e\Delta}{2\hbar} \sum_i T_i \frac{\sin\phi}{\sqrt{1 - T_i \sin^2(\phi/2)}}. \tag{7.4}$$

This "current-phase" relation, linking the supercurrent I to the "phase shift ϕ" across the ballistic weak link is a characteristic of Andreev processes and more generally will be the fingerprint of any superconducting weak link (Golubov et al. 2004). From that last formula, one can see that the "critical" current I_c, defined as the maximum supercurrent that can flow through the weak link with a length shorter than the superconducting coherence length, is quantized. Its maximum value is equal to

$$I_c = \frac{Ne\Delta}{\hbar}. \tag{7.5}$$

In the case of a nanodevice that can be modeled by N ballistic conduction channels placed in parallel, the quantum interference of the Andreev electrons bouncing back and forth between the two S/N and N/S serial interfaces at the junction boundaries is also at the origin of resonance currents called "Multiples Andreev reflections" (Klapwijk et al. 1982), which occur at voltages below the superconducting gap Δ (see examples in Figure 7.18). Due to resonating energy conditions they occur at bias

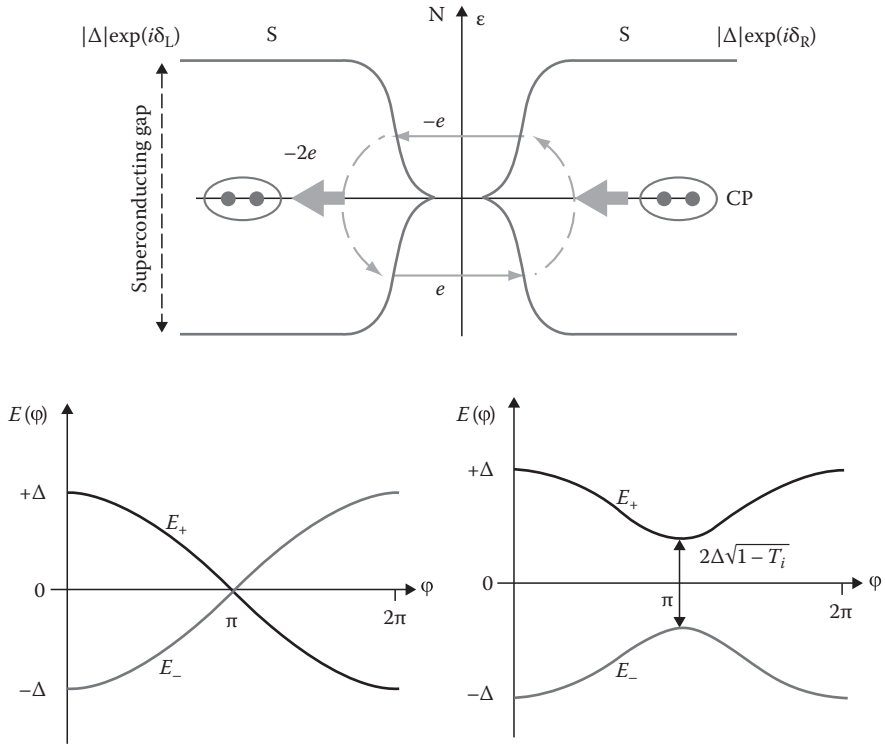

FIGURE 7.3 Top: Schematics depicting superconducting transport through a normal weak link N sandwiched between two superconducting electrodes. An electron is reflected as a hole at the interface with the left superconductor and the hole is reflected back as an electron on the right interface. The net result is a transfer of one Cooper pair through the S/N/S junction. Bottom: Phase dependence of the Andreev bound states energy levels ($\pi=\delta_r-\delta_l$). Left: For a perfectly transmitted channel without scattering potential ($T_i = 1$). Right: For a partially transmitted channel $T_i < 1$. The lower energy state is the only occupied state at low temperature.

voltages corresponding to the sub-harmonics of the superconducting gap ($1/n^*(2\Delta/e)$), where n is an integer. These multiple Andreev Reflections, which position are independent of the weak link density of state but are strongly affected by scattering, will then provide the most convincing experimental signatures of a ballistic weak link.

7.2.6 Introduction to Low-Dimensional sp² Carbon Structures

Low-dimensional allotropes based on carbon nanostructures with sp²-hybridized bonds (Figure 7.4a), such as CNTs, graphenes, and fullerenes, have been extensively studied in the last decade (see appropriate chapters in the Handbook for immediate reference). Their exceptional electronic properties could provide alternative solutions in many fields of electronics including industrial applications for logic. They also behave as ideal media for transmitting superconducting charge carriers for several reasons.

First, they experimentally provide a quasi-perfect crystalline semiconducting lattice on a rather large scale length (typically a fraction of a micron, which corresponds to several thousands of C–C sp²-hybridized bonds in every direction). Second, the inertness and absence of dangling bonds on the carbon surface solves the problem of surface termination (passivation), which is usually found in almost all other systems including all semiconductors candidates. This allow to make atomically clean edges and boundaries. This important feature enables the fabrication of reliable nanoscale metal/sp² carbon contacts with reproducible transparency.

7.2.7 Gate Control of the Weak Link Transparency

As we will detail in the following paragraph, the quantum confinement created by the low dimensionality of carbon nano-objects is at the origin of a sharp dependence of the electron density of states with the chemical potential of the weak link (Figure 7.4a). The resulting Andreev bound states will then be directly affected by this confinement and will create gate-tunable "filters" for the coupling between the two superconducting electrodes (Figure 7.4b). In the superconducting state, a supercurrent will flow if an Andreev bound state is aligned with respect to the Fermi level of the leads as depicted in paragraph 7.2.5. A voltage V_g applied on an electrostatic gate allows for a shift in the chemical potential of the weak link, which is equivalent to translating the confined energy levels (Figure 7.4b) with respect to the Fermi level of the leads. This will in turn tune the maximum superconducting current through the junction, thus implementing a "gate tunable Cooper pair filter." In the following section, we provide details of the typical cases for the different types of nanocarbon structures considered.

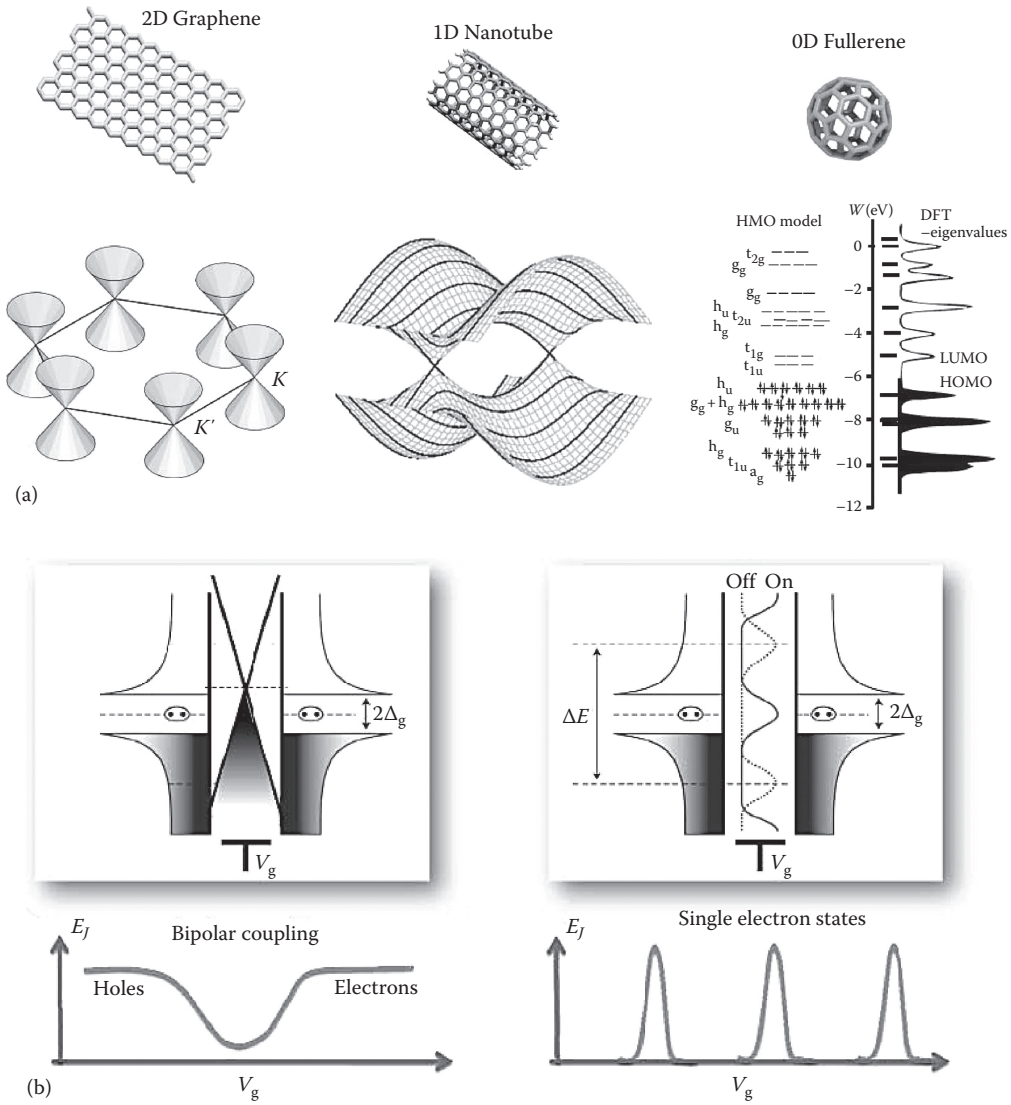

FIGURE 7.4 (a) Crystalline structure of the three low-dimensional phases of sp^2 carbon allotropes (top), and its associated densities of states (bottom). Left: in Graphene, the two dimensional density of states is described by a set of two "Dirac" cones that intersect the Brillouin zone at points *K* and *K*'. These cones provide a linear gap-less dispersion curve. Middle: Metallic single-walled carbon nanotube. The periodic boundary conditions generated by the rolled-up graphene sheet generate solutions symbolized by thick black lines. For selected chiral angles and diameter of the nanotube, these lines intersect the *K* and *K′* points of the Brillouin zone, leading to metallic nanotubes which behave as perfect 1D channels. Right: C60 and derivated fullerenes. The energy spectrum shows discrete states, whose positions could be derived through molecular orbitals (HMO, left side) or density functional theory (DFT, right side of axis). The molecule shows a gap between the occupied and empty states of about 1 eV. (b) "Semiconducting" representations of the energy levels of a Superconductor/Nano-carbon/Superconductor junctions for two dimensional (left) and zero dimensional (right) weak links. The chemical potential of the weak link can be translated by adjustment of a gate voltage V_g which allows to tune the transmission of the Cooper pairs through the weak link. Left: For a 2D junction (i.e., graphene-based weak links), the transport of Cooper pairs can either be transmitted by the valence or the conduction band, leading to an ambipolar semiconductor-like transmission function. At the charge neutrality point (position where the valence and conduction cones intersect, superconducting transport is minimal and is mediated through evanescent waves. Right: for a quantum dot junction (short nanotube junction or fullerene), superconducting transport occurs when a single electron or single hole energy levels is aligned with the Fermi level of the electrode. Such discrete energy spectrum of the weak link acts as a tunable filter for superconducting transport and leads to a series of peaks in the gate dependence of the maximum superconducting current.

7.3 Superconducting Transport in a Carbon Nanotube Weak Link

7.3.1 Introduction to Carbon Nanotube Devices

CNTs are cylinders of carbon of about one nanometer in diameter and up to several micron in length, which can be seen as a rolled-up sheet of sp^2 carbon "graphene." Their cylindrical shape and original 1D electronic structure (for a review, see Charlier et al. 2007) constitute the unique experimental realizations of a quasi-perfect 1D electronic system.

Depending on the chiral angle of the crystalline direction with the cylinder axis, CNTs can exhibit either metallic or semiconducting properties. For the sake of simplicity, one assumes in the following that the nanotube is single-walled and is of a metallic variety (Figure 7.4).

In practice, semiconducting nanotubes are so heavily doped by the metal contacting electrodes that they can also behave in a similar fashion.

A metallic single-walled CNT has two channels of conduction electrons available for electron conduction. According to the Landauer Formula (see Equation 7.3), when perfectly connected to a normal state electrode, it has a resistance that equals the fundamental constant called resistance quantum $h/4e^2 = 6.5\,\mathrm{k\Omega}$. Due to the mismatch of the electron orbitals in the nanotube and in the metal electrodes, the transmission is generally not perfect. The result is equivalent to a tunnel barrier at the contact ($T < 1$). This induces a probability of transmission between the electrode and the nanotube that can be less than unity. These two semi-transparent electronic junctions placed in a series are in all means reminiscent to what is occurring for photon beams in a "Fabry–Perot" cavity (Liang et al. 2001) in which a photon is trapped between two semi-reflective mirrors. Such a cavity has internal resonating modes that correspond to stationary waves given by integer multiples of the half-wavelength and the resonating mode width (invert of the so-called finesse of the cavity) increases linearly with the mirror transparency. Similarly, the CNT junction behaves as a "quantum dot" that the gap between levels (normal modes) increases proportionally to $1/L$ where L is the nanotube length. The width of the levels is proportional to the transmission of contacts. For a short nanotube junction, we obtain discrete levels when the nanotube is completely decoupled from the electrodes like the energy level of an isolated molecule (see the case of C60 Figure 7.4a). These levels widen a bit when the quantum dot interacts with contacts. The position of the nanotube levels with respect to the energy level of the contacts can be adjusted by varying the electrostatic voltage applied to a gate electrode. The transmission of electrons is maximal when the energy level of the quantum dot coincides with the contacts. It thus realizes a molecular transistor (Figure 7.9, left) in which junction transparency can be periodically tuned with a voltage applied to the electrostatic gate (Figure 7.6).

7.3.2 Experimental Realizations of Carbon Nanotube Weak Links

Progress in the late 1990s in improving the contact of CNTs to superconducting electrodes showed that such junctions can exhibit superconducting fluctuations that can be gate controlled (Morpurgo et al. 1999) and that they can accommodate a superconducting current (Kasumov et al. 1999). In 2006, it was then shown that such junctions behave as gate-controlled Josephson junctions (Jarillo-Herrero et al. 2006, Jørgensen et al. 2006). During this period, fabrication techniques have been optimized to generate low-resistive contacts at the metal/sp^2 carbon interfaces. They required the use of specific metals for connection such as titanium (Jarillo-Herrero et al. 2006) or palladium (Cleuziou et al. 2006, Javey et al. 2003) that both provide good wetting properties onto the sp^2 carbon layer and minimize the Schottky barrier that could arise from the differences of the electronic work functions at the metal/carbon interface. More subtle effects linked to the hybridization of the metal orbitals to sp^2 carbon (Nemec et al. 2006) could explain the differences

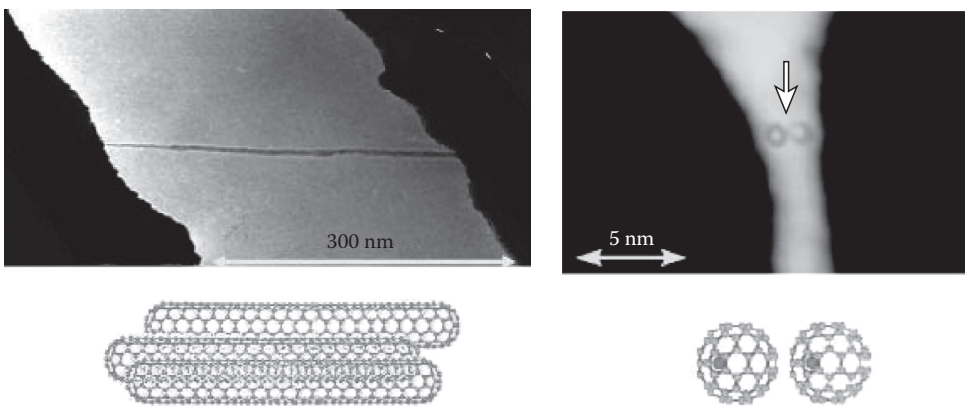

FIGURE 7.5 Micrographs made using a transmission electron microscope (TEM) of superconducting junctions, involving a carbon nanotube bundle, left and for a fullerene dimer formed by two C82 molecules in series, right. The weak links are free-standing over a slit and bridge superconducting electrodes deposited on a silicon membrane. This allows TEM imaging and electrical measurements on the same samples. (After Kasumov, A.Y. et al., *Science*, 284, 1508, 1999. With permission.)

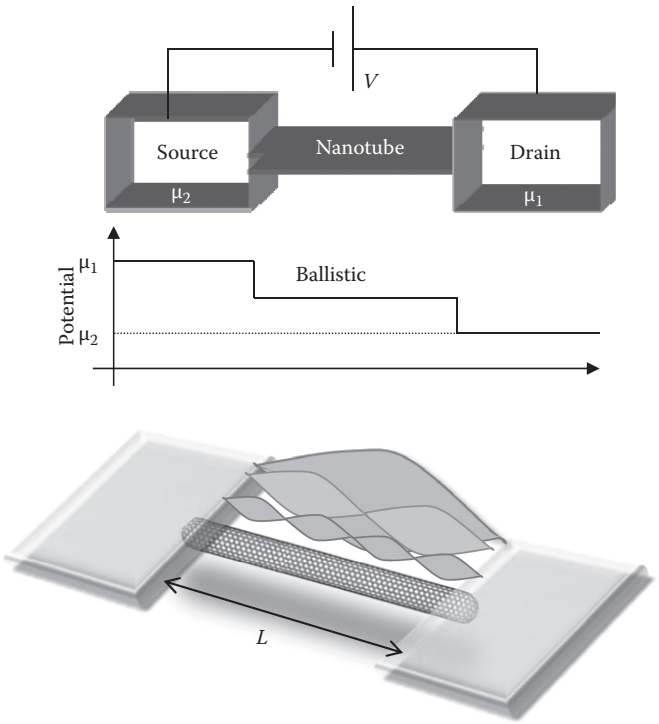

FIGURE 7.6 Top schematic of electron transport through a "defect-less" carbon nanotube contacted with two metallic electrodes. Electron transport is ballistic along the nanotube: the voltage drop $V = \mu_1 - \mu_2$ is occurring at the metal/nanotube contacts which act as tunnel barriers partially transmitting the electron. Bottom: For low resistance barrier contacts, the device act as a Fabry–Perot interferometer in which standing electron waves are separated by the energy difference $\Delta E = h v_F/2L$.

of interface resistances that have been reproducibly observed between these different metals (see Figure 7.7).

While not superconducting by itself, the Pd or Ti interfacing layer is made thin enough (a few nanometers) so that it lets the superconductivity induced by a covering top layer made of aluminum (Jarillo-Herrero et al. 2006) or niobium (Pallecchi et al. 2008) establish through the whole sandwich by the proximity effect. Using those materials, high transparency contacts with almost transparency T close to unity (Javey et al. 2003) can be reproducibly achieved by metal evaporation thus placing connected nanotube junctions in the high coupling limit (Liang et al. 2001). Advances in synthesis methods of nanotubes (in situ grown by CVD), which allow nanotubes to be connected during their growth onto platinum contacts (Cao et al. 2005) are another promising fabrication route. This last method makes clean suspended nanotube junctions, which in the near future could make possible the coupling of nanomechanical vibration modes to superconducting charge transport, as has been recently observed with normal charge carriers, by using non-superconducting metal electrodes as contacts (Lassagne et al. 2009, Steele et al. 2009).

7.3.3 Nanotube Quantum Dot Connected to Superconducting Electrodes

In a CNT weak link, the device considered is a portion of a nanotube with a length L connected by the two superconducting contacts (see Figure 7.8).

At one dimension, a defect along the channel cannot be overcome by the diffusion of the incoming electrons like it occurs in a 2D or 3D system. Therefore, the slightest defect along the nanotube generates back scattering which cancel the transmission of a supercurrent by Andreev bound states. It is then extremely important to realize the injection of Cooper pairs in a perfectly clean system. The nanotube portion length L is usually chosen not to exceed 300 nm in order to limit the occurrence of these structural defects. In such a case, a ballistic transport is reached (i.e., the voltage drop is localized at the contacts, see the top of Figure 7.6). The sub-micron length and nanometer diameter of the nanotube junction makes the intrinsic capacitance C of the junction very small, creating a Coulomb blockade effect (Beenakker and van Houten 1992). A charging energy $e^2/2C$ contributes to their energy and adds to the kinetic energy which leads to the Andreev bound states becoming

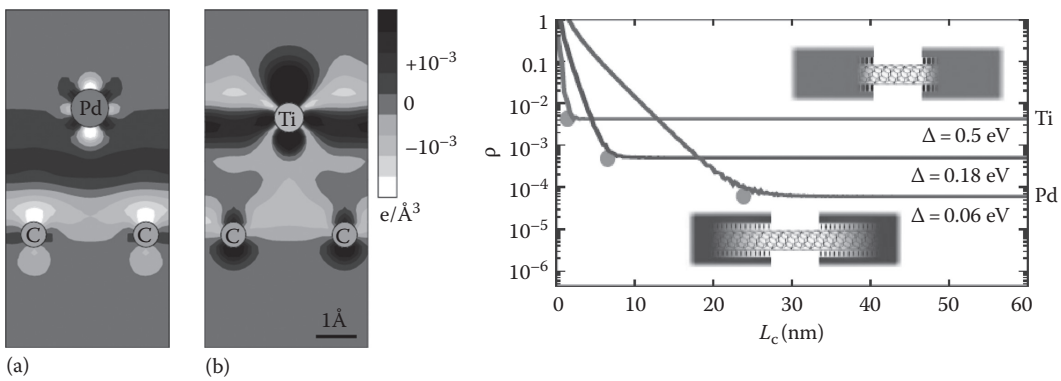

FIGURE 7.7 Left: Cross section showing the charge density redistribution at a metal/carbon nanotube interface for Palladium (a) and Titanium contacts (b). These results are obtained using an ab-initio density functional theory. The titanium contact show a much stronger hybridization with the carbon surface compared to Palladium. Right: Contact reflection coefficient $r = 1 - t$, (where t is contact transmission) as a function of the contact length L_c, the transparency first increases linearly with the contact length then saturates at a constant value independent on the contact length. Their results shows that the optimal metal/carbon interface transparency is obtained for a contact combining low hybridization with a large contact length. (Adapted from Nemec, N. et al., *Phys. Rev. Lett.*, 96, 076802, 2006. With permission.)

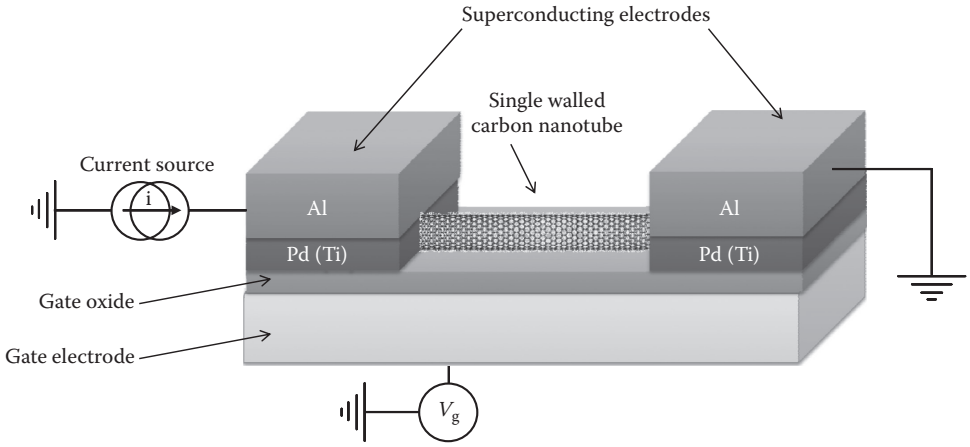

FIGURE 7.8 Schematic diagram of a carbon nanotube superconducting transistor. The contacting electrodes are made of a bilayer of aluminum (for the source of superconductivity) and underlayer of few nanometer thick film either made of palladium or titanium to increase contact transparency. These latter materials are known for their good contact abilities on sp^2 carbon layers (see Figure 7.7). The highly doped silicon substrate is connected to a voltage source V_g and is used as a "backgate" electrode.

$$E_{e,h} = \frac{e^2}{2C}(\pm 1 - n_g)^2 \pm \hbar v_F k, \tag{7.6}$$

where n_g is the gate-induced charge on the nanotube [$n_g = C_g V_g/e$]; electrostatic degeneracy between charge states occurs at zero gate bias.

The wavevector k is quantized by the Andreev boundary condition at the superconducting interfaces in multiples of $1/L$. In the presence of the Coulomb repulsion in the Quantum dot, the Andreev bound states described in Section 7.2.5 split their energy in a sum of the charging energy term and the confinement energy term, which for the electron states give

$$E_e = \frac{e^2}{2C}(1 - n_g)^2 + \frac{\hbar v_F T}{2L}(\phi + \psi_e(n_g, \phi)), \tag{7.7}$$

and for hole states

$$E_h = \frac{e^2}{2C}(1 + n_g)^2 + \frac{\hbar v_F T}{2L}(\phi + \psi_h(n_g, \phi)), \tag{7.8}$$

where $\psi_h(n_g,\phi)$ is a gate-dependent phase. In most experiments, the charging energy e^2/C and quantization energies are of the same order of magnitude (typically 1–10 meV). The eigenstates are then mixed states of charge and Andreev bound states. Close to a degeneracy point (n_g=1/2), the CNT Andreev bound states become resonant with the Fermi level of the leads, thus maximizing the supercurrent flow. As this energy separation can be tuned by applying a gate voltage V_g to the nanotube, we are able to tune the maximum supercurrent (referred to as "switching current") with the gate voltage.

The gate dependence of this last quantity is then periodic (see Figure 7.9, left) and directly reflects the conductance variations observed in the normal state (linked to the Fabry–Perot-like oscillations described in the previous paragraph). By varying the electrostatic voltage V_g applied to the nanotube, it is possible to shift the position of these energy levels relative to the energy levels of the electrons in superconducting contacts (Figure 7.4b, right). When levels coincide, the maximum supercurrent that can pass before obtaining a resistive state (called "current jump") reaches its maximum. On the opposite, if Andreev bound states spectral weight decrease due to levels misalignment, the current will then be minimal. It has been shown (Cleuziou 2006) that even in the case of abscence of Andreev bound states, a tiny supercurrent (of the order of tens of pico-amperes) can be maintained through the CNT probably due to higher order cotunneling processes. It has been experimentally shown by Jarillo-Herrero et al. (2006) that the maximum superconducting current can indeed be controlled by the gate voltage (Figure 7.9).

Therefore, such CNT junctions implement superconducting transistors for which the switching current can be tuned with the gate voltage over a large dynamic range (typically up to 2–3 orders of magnitude, depending on the coupling; see Figure 7.9 right). The current–voltage curves show some marked hysteresis especially in the off-state. The origin of this hysteresis (Gang et al. 2009), which is usually attributed to the existence of a capacitance in parallel with the junction for tunnel weak links (Barone and Paterno 1982), is still debated in the case of these carbon weak links in which the capacitance is extremely small. Hysteresis could rather be associated with the Joule dissipation that occurs in the weak link after switching to the normal state as it has been recently observed in metallic junctions (Courtois et al. 2008). Heat dissipation within the tiny volume of the junction could delay the re-trapping of the weak link in the superconducting state once the current bias is decreased. This occurs especially when the nanotube is in the high resistance state (Off State, see Figure 7.9).

The maximum superconducting current that can be carried by a single-walled CNT is given by Equation 7.5 and is equal to $2\Delta/\hbar \sim 30$ nA for the two conducting channels of a metallic

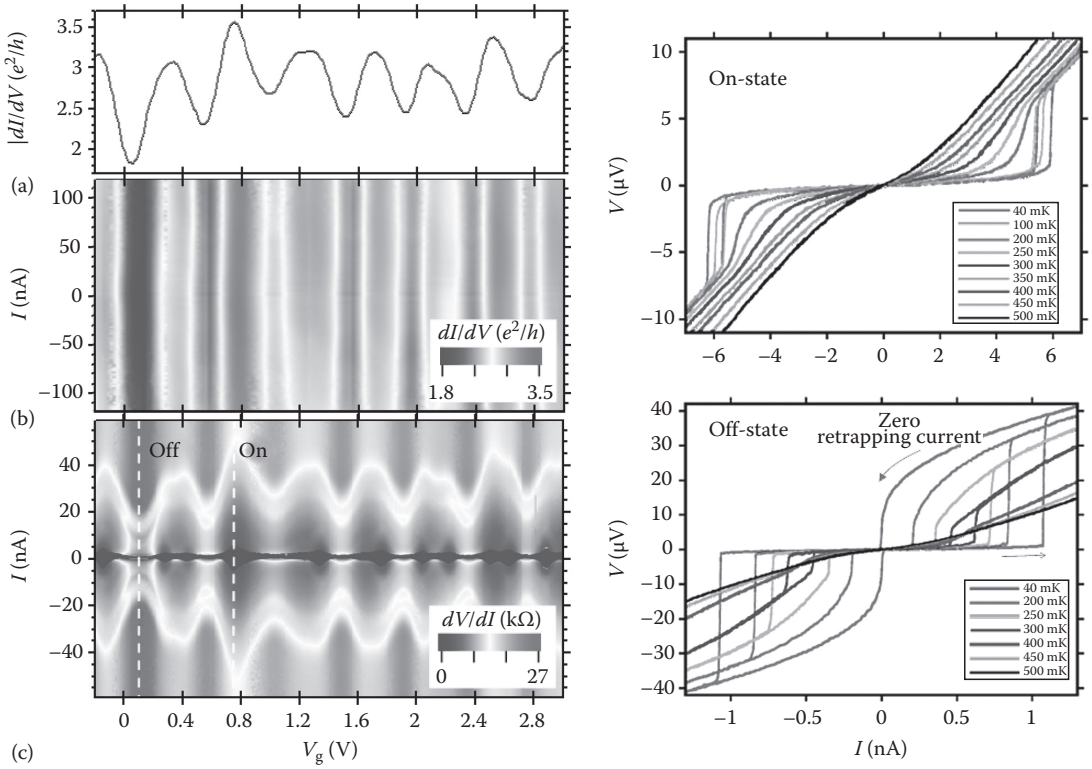

FIGURE 7.9 Electron transport through a transparent carbon nanotube junction as a function of the gate-voltage V_g. Top left: (a) Gate modulation of the nanotube conductivity dI/dV at zero bias in the normal state. (b) Map of the conductivity for current bias I. At resonance, the nanotube conductance is close to the theoretical maximum $4e^2/h$ thus corresponds to the high transparency limit ($t \sim 1$). Gate oscillations are broadly distributed in gate due to the strong hybridization of the nanotube levels with the contacting leads. (c) Differential resistivity dV/dI versus current I and V_g in the superconducting state. Darkest zones around zero bias corresponds to the supercurrent flow which are occurring to the same gate voltages as the high conducting state for non-superconducting electrodes. Right column: Voltage–Current characteristics of a carbon nanotube superconducting transistor measured at low temperature, showing a modulation of the superconducting current for gate voltage corresponding respectively to the on and off state (depicted by the white dotted lines on the resistance map shown in left). The off-state show a strong hysteresis which completely vanished in the on-state.

single-walled CNT connected to Aluminum electrode. In early experiments, measured switching currents were of a few nanoamperes, typically 10%–20% of the expected value. The discrepancy between the predicted and the observed values have been attributed to the sensitivity of the superconducting current to external perturbations, such as micro-wave photons emitted by thermal fluctuations and traveling along the lines. A better control of the electromagnetic environment by using LC and RC filtering on the measurement lines (Jarillo-Herrero et al. 2006) and by implementing locally dissipative elements, such as on-chip resistors close to the nanotube junctions (Jorgensen et al. 2007), has proven to be helpful to stabilize the superconducting current and increase the measured value of the switching current.

7.3.4 High-Frequency Irradiation of Nanotube Weak Links

According to what is known as the AC Josephson Effect, the phase twist across the weak links varies in time at the frequency given by the characteristic frequency of the coupling. Upon irradiation with radio frequency (RF) electromagnetic waves (Barone and Paterno 1982), superconducting weak links are known to develop a series of voltages steps that are so precisely positioned that they are used to define the voltage standards (Hamilton 2000). In the case of the irradiation of a single quantum channel, a peculiar behavior is expected for the RF-irradiated Andreev states (Averin and Bardas 1995).

Experimental measurements (Cleuziou et al. 2007) showed that the voltage steps across the nanotube weak link follow a completely different behavior upon the RF irradiation power depending on if the nanotube is placed either in the "on" or "off" state (see Figure 7.10). This behavior appears to be linked to the existence of the hysteresis found in the direct current (DC) measurements (Figure 7.9) and is discussed in the previous paragraph. They have been associated with the change of dissipation (Liu et al. 2009) that occurs when the nanotube levels are aligned or misaligned with the level of the leads. The RF properties of the superconducting carbon-based junction is expected to be very interesting principally because of their tiny size, which induces an extremely low intrinsic capacitance C, thus leading to extremely high cut-off frequencies $(RC)^{-1}$ that could exceed tens of GHz (Burke 2004). The coupling of these weak links to superconducting resonators will allow for the assessment of their additional RF properties in the near future.

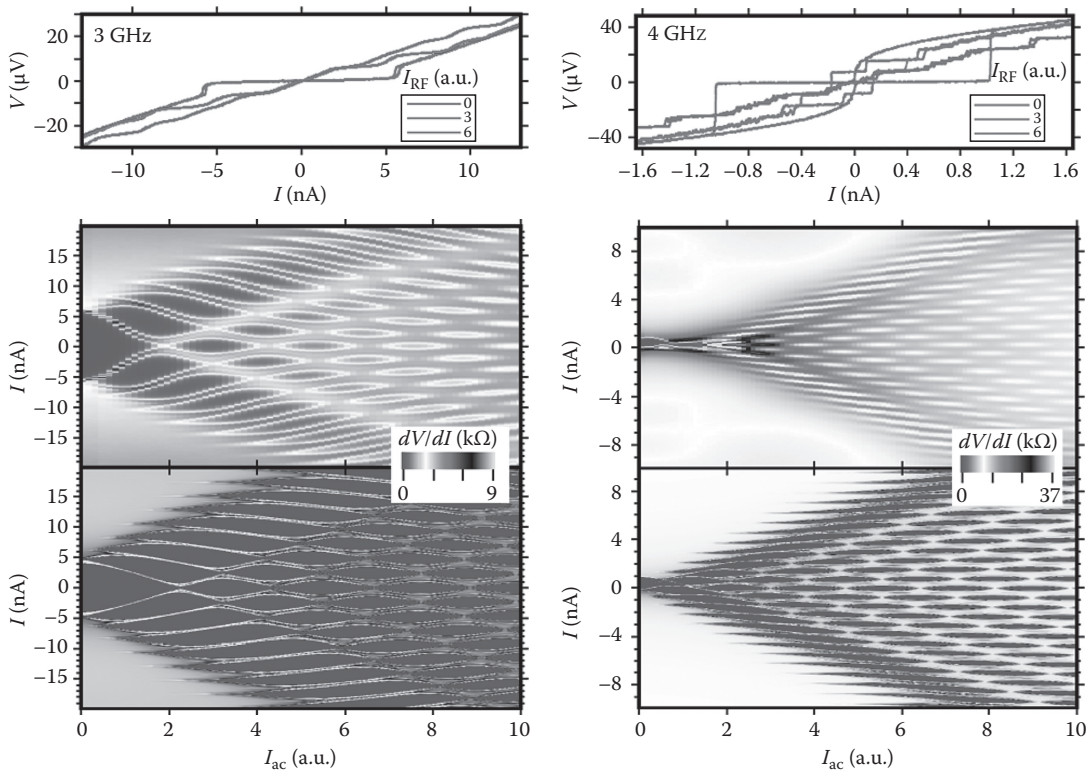

FIGURE 7.10 Carbon nanotube superconducting transistor behavior upon radio-frequency (RF) irradiation in the on and off state (respectively shown in the left and right columns). Top curves: Voltage current characteristics at several RF amplitudes showing the typical constant voltage steps, known as "Shapiro steps." Hysteresis in these steps is seen on the "on" state and vanishes in the "off" state. Middle panels: differential resistance *dV/dI* maps for increasing RF power showing a different behavior in the off and on state. Bottom panels: Numerical simulation of the data of the middle panels using the RSJ (resp. RCSJ) non linear model for the on (resp. off) states.

7.4 Nanotube-Based Superconducting Quantum Interferometers

7.4.1 Quantum Interference with Single Nanotube Weak Links

An interferometer is an apparatus that measures the phase differences between two wave components. Interferometers work by splitting a wave into two components, sending them off along different paths, and then recombining them to record an interference pattern. The pattern is dependent on the phase difference arising from changes in the conditions along their paths. A superconducting interferometer (referred to by its acronym "DC-SQUID" [Clarke and Braginski 2004], which stands for direct current superconducting quantum interferometer device) achieves a kind of "Young slits" experiment with Cooper pairs, the slit being implemented by 2 weak links placed in parallel.

The coherence of the photon beam is provided here by the coherence of the Cooper pair supercurrent. Such a device was first implemented in the 1960s by using oxide-based tunnel weak links (Jaklevic et al. 1964), which rapidly became ubiquitous in the field of superconducting electronics: SQUIDs have been successfully used as ultra-sensitive magnetometers as well as amplifiers of low-level signals and low-impedance sources (Clarke and Braginski 2004).

The main feature of this device is that the maximum superconducting current can be periodically modulated by a tiny magnetic flux threaded by the loop, with a period equal to the flux quantum $\phi_0 = h/2e$ (Figure 7.11, right). We briefly recall in the next paragraph the principle of operation of a DC-SQUID.

The two currents circulating in each weak link interfere with each other and each weak link induces a phase shift $\Delta\phi_i$. according to Equation 7.2.

The total supercurrent is therefore written as the sum of two currents flowing in each branch.

If one assumes a sinusoidal current-phase relation, one obtains

$$I = I_{c1}\,\sin\left(\Delta\phi_1\right) + I_{c2}\,\sin\left(\Delta\phi_2\right). \tag{7.9}$$

Furthermore, an additional controlled phase (analogous to a geometric phase) can be introduced by applying a magnetic flux Φ_{ext} through the loop formed by the two weak link branches. Because of the uniqueness of the superconducting wave function, Φ_{ext} couples the phase shifts induced by each of these junctions in the two branches

$$2\pi\left(\frac{\Phi_{ext}}{\Phi_o}\right) = \Delta\phi_1 - \Delta\phi_2\ (\mathrm{mod}.2\pi). \tag{7.10}$$

In practice, the SQUID is current-biased and one measures the maximum superconducting current before the onset of a finite voltage

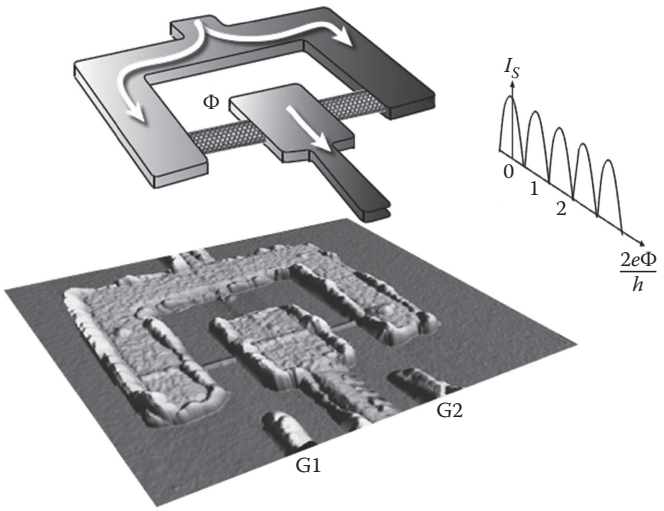

FIGURE 7.11 Schematic diagram of a superconducting quantum interferometer (SQUID) based on carbon nanotube weak links (top) aligned with an atomic force micrograph of a real device. (Adapted from Cleuziou, J.-P. et al., *Nat. Nanotechnol.*, 1, 53, 2006.) Thanks to a peculiar fork geometry design, the weak links in each branch can be made of two portions of the same carbon nanotube generating two independent quantum dots. The phase shift between the two currents flowing in each arm (white arrows) is adjusted by the magnetic flux *F* threaded by the loop. The two electrodes, G1 and G2 allow the application of locally addressed gate voltages which tune independently the transparency of each portion of the nanotube according to the principles of the carbon nanotube junctions shown above.

across the device. This switching current is directly related to the critical current of the SQUID, which can be obtained by computing the maximum value of the solutions of Equations 7.9 and 7.10.

$$I_c = \sqrt{\left(I_{c1} - I_{c2}\right)^2 + 4I_{c1}I_{c2}\cos^2\left(\frac{\pi\Phi_{ext}}{\Phi_o}\right)}. \qquad (7.11)$$

Due to thermal or quantum fluctuations of the phase across the weak links, the measured switching current does not reach that critical value I_c but its magnetic flux dependence still follows the relation in Equation 7.11. The quantum interference, therefore, produces periodic oscillations of the current as a function of external magnetic flux, analogous to the bright fringes observed in an experiment of Young's slit and whose period is equal to the flux quantum $h/2e$.

At the nanometer scale, a single CNT can be used to implement the two weak links that are placed on both arms of the interferometer by using a forked geometry (Figure 7.11).

The two branches implement two nanotube quantum dots; their behavior has been detailed in Section 7.3.3. It is therefore possible to modulate the quantum interference by independently adjusting the intensity of coupling in each quantum dot (see the three limit cases in Figure 7.12). Such electrostatic control of a DC-SQUID is extremely useful, both to optimize its operation and its coupling to local magnetic fields to study the detailed physics of the molecular Josephson junction. More generally, it is an experimental model system for the study of the variation of the phase of charge carriers across a quantum dot. Many physical phenomena such as an equal number of electrons in the nanotube (including those related to interactions between the spins of electrons) have been predicted and may now be studied.

The integration of these nanotubes between superconducting electrodes opens the way for the realization of superconducting circuits operating at radio frequencies, particularly useful to follow the time evolution of magnetization of individual nanoobjects. They could afford to explore how quantum states of magnetization of a molecule magnet can couple to those generated in a superconducting circuit (which are the basis of superconducting quantum bits).

7.4.2 Tunability of the Phase Shift across Nanotube Weak Links

For an odd electron number of charge sitting on the nanotube, a CNT weak link can behave as a quantum dot that has a nonzero spin state. It thus behaves as a "spin impurity" seen from the superconducting electrodes. Quantum dots populated with a odd number of electrons are prone to an additional electronic resonance called the Kondo Effect (Kouwenhoven and Glazman 2001). This resonance originates from the tendency of conduction electrons to screen the nonzero spin states of the quantum dot in a similar fashion as it occurs in a 3D metal, which contains a low level of magnetic impurities. This screening current adds to the usual conduction channel of the quantum dot and generates a conduction channel at zero bias, which bypasses the Coulomb blockade regime (Nygard et al. 2000). In the superconducting state, the nonzero spin tunneling induces higher order electron transfers events (Buitelaar et al. 2002) that allow the flipping of both spins of the Cooper pair during the tunneling through the nanotube. This amounts to changing the sign of the Cooper pair wave function. As can be seen in Equation 7.1, a change of sign in this wave function is equivalent to a phase shift of π in the superconducting phase.

Such an effect, in which the minimum energy state of one of the Josephson junctions (the so-called π-junction) is obtained for a phase difference of π instead of 0, has been the focus of intense studies. Reminiscent of ferromagnetic impurities in a Josephson junction, it was predicted some 20 years ago (Glazman and Matveev 1989) that a reverse Josephson current would take place in a junction involving tunneling through a quantum dot populated with an odd number of electrons. For a strong Kondo effect (Figure 7.2), the Josephson coupling is expected to be positive (0-junction) since the localized spin is screened due to the Kondo effect. On the other hand, for a weak Kondo effect, the large onsite interaction only allows the electrons in a Cooper pair to tunnel one-by-one via virtual processes in which the spin ordering of the Cooper pair is reversed, leading to a negative Josephson coupling (π-junction) and hence a reversed supercurrent. Controlling the phase-shift across a nanotube weak link can be achieved by tuning the charge induced on the weak link (see Figure 7.13).

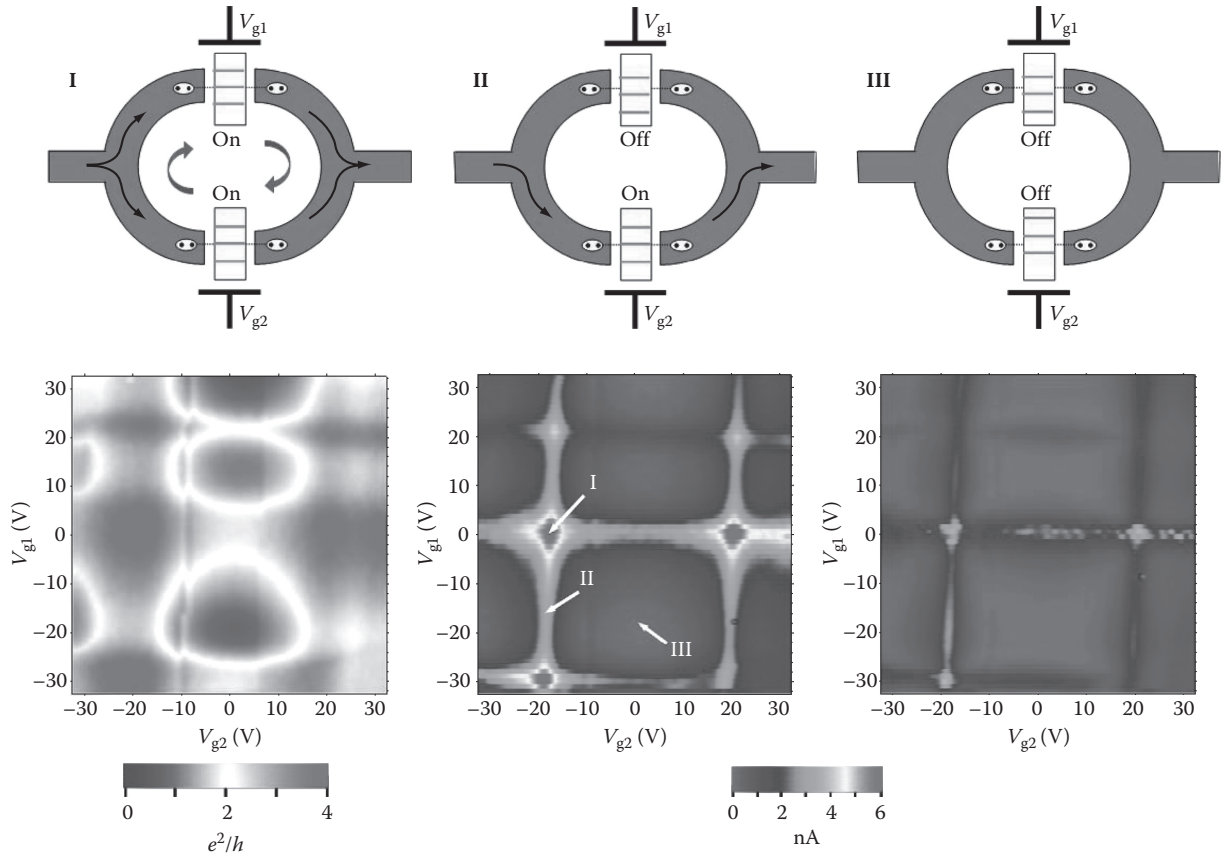

FIGURE 7.12 Schematics of three typical working points of a carbon nanotube SQUID, in case **I**, both junctions have a quantum level adjusted to the Fermi energy of the leads (on-resonance) and supercurrent can flow through the device. In **II** and **III**, one and two junctions are tuned off-resonance, respectively. (Adapted from Cleuziou, J.-P. et al., *Nat. Nanotechnol.*, 1, 53, 2006. With permission.)

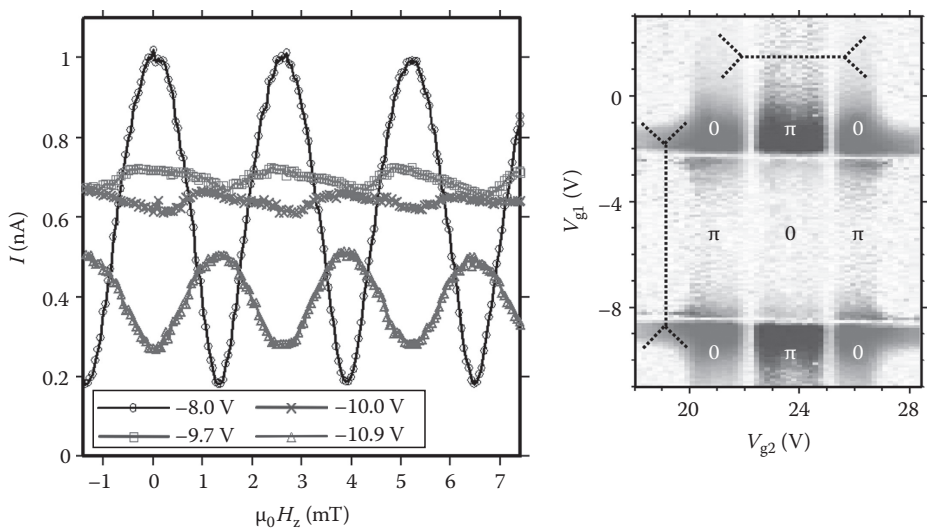

FIGURE 7.13 Gate control of the phase in a carbon nanotube SQUID. Left: magnetic field dependence of the maximum supercurrent in a nanotube SQUID as a function for different lateral gate voltages V_g, the modulation can be tuned from an even (0-junction SQUID) to an odd (π-junction SQUID) curve. The modulation is highly non-sinusoidal between the two states (Right), Color-scale representation of differential resistivity dV/dI as a function of the lateral gate voltages V_{g1} and V_{g2} showing the periodic switching between zero and π modulation. The dotted lines corresponds to voltage gate range for which an odd number of electrons is in the quantum dot. Note that when both SQUID junctions has π modulation, the SQUID recovers normal (0) modulation. (Adapted from Cleuziou, J.-P. et al., *Nat. Nanotechnol.*, 1, 53, 2006. With permission.)

7.4.3 Application of Nanotube Weak Links to Magnetometry

SQUID-based magnetometry in the near field regime (i.e., for the detection of fields emitted by source at the distance smaller than the SQUID loop radius) has been exploited for nearly 15 years in the field of molecular magnetism (Wernsdorfer 2001). It is based on the inductive coupling of a nano-magnetic object placed near a constriction of the loop of a SQUID. A local change in flux, for example, induced by the magnetization reversal of a magnetic dipole in the vicinity of the loop (Wernsdorfer et al. 1995) will be detected by a variation in the SQUID switching current. By recording these changes while sweeping the magnetic field in direction and intensity, one can accurately study the physical conditions of magnetization switching of a nanoparticle or a assembly of molecules. Therefore, it is possible to study the details of the dynamics of magnetization reversal on nano-magnets and highlight, in the case of molecular magnets, the existence of a tunnel effect of this reversal (Wernsdorfer et al. 1997).

The current system is limited in sensitivity and the threshold corresponds to the detection of a few thousands of elementary spins. The miniaturization of the most sensitive SQUID (superconducting weak seal, represented here by the CNT) seems to be a promising way of gaining sensitivity.

The strong 1D geometrical form factor of CNT junctions combined with their tiny cross-section open some interesting perspectives concerning the magnetometry at the nanometer scale. Indeed one can show that shrinking the cross-section of a weak link allows for the optimization of the inductive coupling between the loop of the SQUID magnetometer and a magnetic object sitting in close vicinity of the weak link (Bouchiat 2009). This inductive coupling factor is known to be proportional to the inverse of the weak link cross-section radius. Therefore, miniaturization of the weak link footprint is indeed necessary to match the size of a single molecule magnet (see Figure 7.14).

Noise measurements on practical devices (Cleuziou et al. 2006) have shown that the detection threshold in CNT magnetometers should allow measurements in the near field regime of magnetized nano-objects of typically 10 Bohr magnetons, for example, strays emitted by a single molecular magnet (see Figure 7.14). The control and measurement of the magnetization of a single molecular magnet is indeed a promising way to implement spin Qubits, which are readily interfaced to coherent superconducting electronic currents. The fact that nanotube SQUIDs can see their current gated within a large dynamic from 10 nA down to picoampere critical currents (Cleuziou et al. 2006) (see Figure 7.9) is also a promising feature. This could allow the limiting of the back-action of the measuring instrument to the evolving quantum spin, thus helping to preserve long coherence times. More generally, magnetometers based on these ultra-miniaturized weak links could provide new instrumentation set-ups, useful for the building of a spintronics at the molecular scale (Bogani and Wernsdorfer 2008).

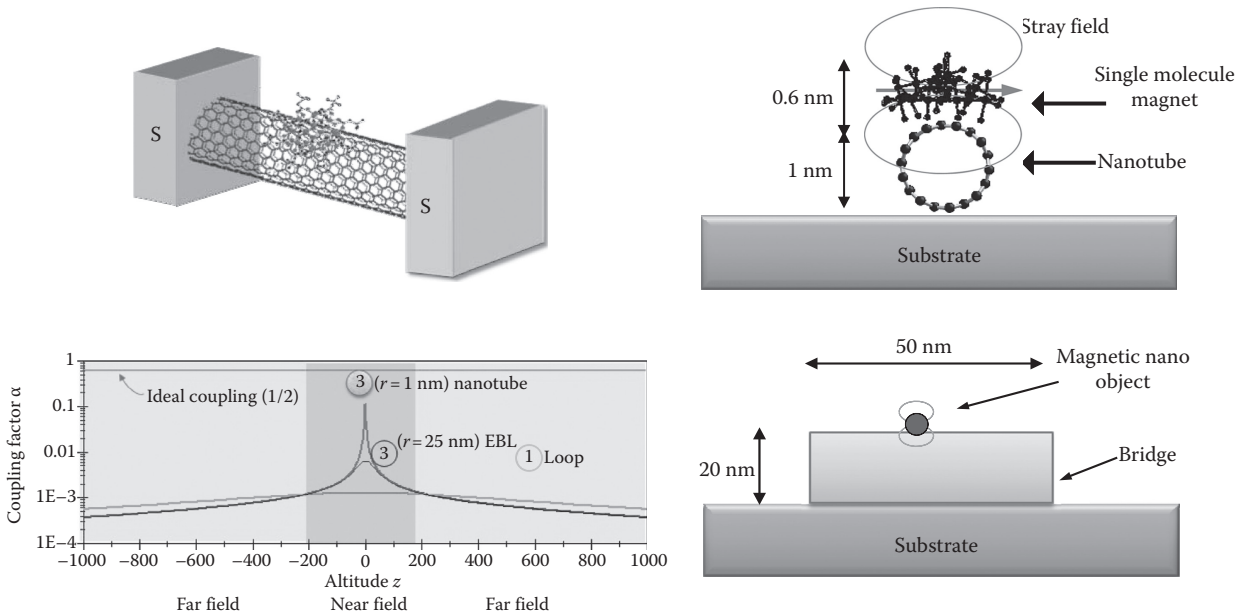

FIGURE 7.14 Optimization of the inductive coupling of single molecule magnet to the nanotube superconducting junction. Top left: artist view of the grafting of a single molecule magnet (here a "manganese-12" molecule) in close contact onto a carbon nanotube junction. Top right, cross section of the same assembly showing the stray field emitted from the magnetic molecule. Bottom right: cross section of a similar situation for the previous generation of weak links made of a nanowire with state-of-the art electron beam lithography. Bottom left: Simulation of the inductive coupling factor α for the two cases shown in right as a function of the distance *z* between the centers of the two coupled objects: the black curve stand for a lithography-made nanobridge ($r = 25$ nm) while the red curve depicts the situation for a single-walled carbon nanotube ($r = 1$ nm) (red curve) The nanotube based weak link which diameter matches the molecule size, better grab the stray field and thus increase the inductive coupling by two order of magnitude with respect to the weak link made by top down lithography. The top straight line depicts the theoretical coupling limit ($\alpha = 1/2$) which is almost reached with a carbon nanotube junction.

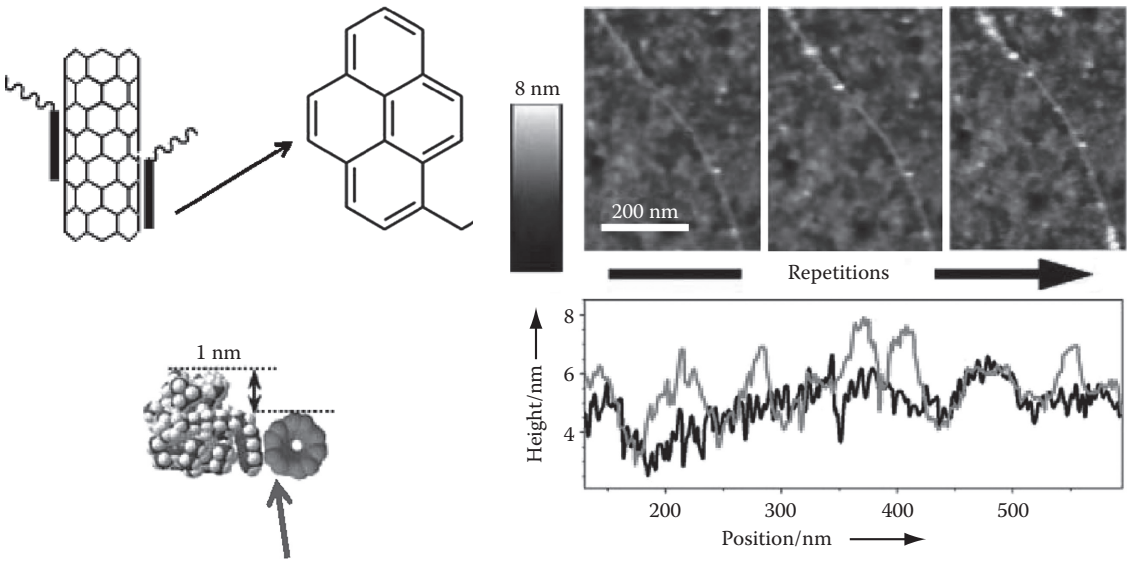

FIGURE 7.15 Chemical functionalization of carbon nanotube weak links for single molecule magnetism applications. Top left: Schematics showing the grafting of carbon nanotubes with organic molecules using pyrene group (inset) that specifically bind onto nanotube side walls by p-p interaction. (After Chen, R. et al., *J. Am. Chem. Soc*., 123, 3838, 2001.) Right: AFM topographic analysis of molecular magnet/nanotube hybrids. Top right: Height images of the same CNT acquired on repeating the grafting process: left one time, center four times, right ten times. Bottom right: Section profile along the same CNT before (black line) and after (red line) multiple graftings of 1. Bottom left: Heights of the grafted objects. (Adapted from Bogani, L. et al., *Angew. Chem*., 48, 746, 2009.)

The full integration of magnetic molecules coupled with the device is still to be made. This requires control of the binding of single magnetic molecules to the nanotube while preserving its good conduction properties. Progress has been made in that direction by using chemically functionalized organic entities (Chen et al. 2001) that can mimic on a few cells, the graphitic honeycomb lattice (pyrene groups, see Figure 7.15), thus through π–π interaction, they provide specific grafting along the nanotube side walls. Pyrene functionalized molecular magnets have been shown (Bogani et al. 2009) to specifically bind in solution in a rather controlled way onto nanotube junctions.

7.4.4 Application of Nanotube Weak Links to Quantum Information

As shown above, CNT-based weak links offer the possibility of realizing the controlled injection of Cooper pairs that travel as

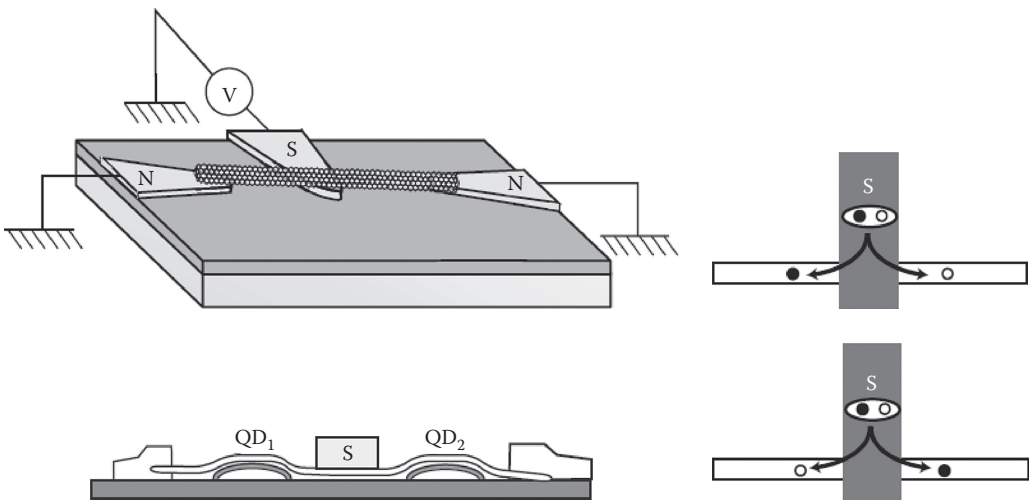

FIGURE 7.16 Top left: Schematics of a carbon nanotube based Cooper pair splitter: the nanotube is coupled in its middle part to a voltage biased superconducting electrode (noted S) which injects Cooper pairs in the nanotube. The nanotube splits the current into two components which are collected by symmetrically positioned normal metal electrodes. Bottom left: Cross section of the same device. The two branches act as nanotube quantum dots noted QD_1 and QD_2 in a similarly geometry as previously presented nanotube SQUID. Right: schematics showing the two possible paths for the two correlated electrons that forms the Cooper pair which splits in the nanotube and travel in opposite directions. (Adapted from Bouchiat, V. et al., *Nanotechnology*, 14, 77, 2003.)

correlated quasi-particles in a 1D or 0D conductor. Many experiments taking advantage of splitting the quantum correlated charge carriers emitted from a superconducting electrode can be devised. They are mostly inspired from those already realized in quantum optics and propose to realize their fully-integrated solid-state counterparts involving Cooper pairs instead of correlated photon pairs. In Cooper pairs splitting experiment, an additional quantum degree of freedom is also provided by the spin of the electron.

Among interesting basic devices is the nanotube-based Cooper pair beam splitter (Figure 7.16). It consists of a single-walled CNT connected at both ends to normal state electrodes and coupled in its middle part to a superconducting nanowire. Such a device acts as an electronic beam splitter for correlated electrons originating from the superconductor. Note that this geometry is very similar to the nanotube SQUID described in Section 7.4, but with the notable difference of having spatially separated normal-state "collecting electrodes" instead of a single superconducting one found in the SQUID geometry (Figure 7.11).

The Cooper pair splitter device was first discussed on a theoretical level in 2002–2003 (Bena et al. 2002, Recher and Loss 2002, Bouchiat et al. 2003) and its first preliminary experimental realizations just appeared recently using either a CNT (Herrmann et al. 2010) or a III–V semiconducting nanowire (Hofstetter et al. 2009).

In this device, the splitting of Cooper pairs in the superconductor provides two electrons with opposite spins. In the case of a full splitting, they can travel into opposite directions in the nanotube and are individually collected at both ends of the nanotube (Figure 7.16). Thanks to the Andreev process, the Cooper pair splitter generates electrons that are simultaneously entangled in energy and in spin. Correlation and noise measurements of the current emerging from the nanotube should allow the testing of Bell inequalities (Bouchiat et al. 2003) with electrons instead of photons.

7.5 Graphene-Based Superconducting Weak Links

7.5.1 Proximity Effect in Graphene Weak Links

Graphene, a single atomic layer of graphite, exhibits unique electrical and mechanical properties on account of its reduced dimensionality and "relativistic" band structure. The transport properties of the graphene sheets have recently received a lot of attention on both experimental (Geim and Novoselov 2007) and theoretical points of view. On one hand, this is due to its 2D character and on the other hand, to its remarkable band structure combining a linear dispersion relation of electronic wave functions similar to mass-less particles and perfect electron hole symmetry. The Fermi surface consists of two cones touching at one singular point, the so-called Dirac point, where the density of states is zero (see Figure 7.4a). Over the last 5 years, graphene has emerged as a unique platform for testing new electronic properties of condensed matter (Figure 7.17).

By tuning a gate voltage positively or negatively, one can respectively induce a finite density of electrons and holes with a linear energy dispersion curve. Furthermore, this 2D electron gas can be exposed to external physicochemical functionalization and be easily connected with superconducting electrodes. Soon after first electron transport measurements, graphene has been shown to allow Cooper pair transport (Heersche et al. 2007) with a well-defined Josephson effect exhibiting microamperes of critical current (Figure 7.18) and clearly defined (Figure 7.18) multiple Andreev reflections (Du et al. 2008a, Heersche et al. 2007).

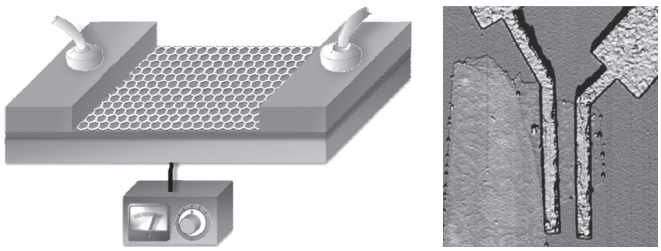

FIGURE 7.17 Left: Schematic diagram of a graphene-based superconducting weak link. The graphene carrier density is controlled by adjusting the backgate voltage on the silicon substrate, which is isolated from the device by a thermal oxide layer. Right: Atomic force micrograph of a first realized graphene superconducting junction. (Adapted from Heersche, H.B. et al., *Nature*, 446, 56, 2007.)

The supercurrent of such a junction can be modulated in intensity with the gate, which tunes the carrier type and density of the graphene sheet (see Figure 7.4b). Depending on the gate voltage applied to the graphene, a supercurrent can be mediated by either electrons or holes (Heersche et al. 2007), which makes graphene the first 2D ambipolar superconducting material. Unlike nanotube weak links, the modulation no more shows any gate periodicy in the modulation of the switching supercurrent because of the absence of lateral quantum confinement. The superconducting current is monotonically increased by increasing the gate and, as it is predicted by the number of conduction channels contributing in parallel to the superconducting current (Equations 7.4 and 7.5), the intensity of the maximum superconducting current is usually thousands of times the one measured for a CNT junction.

New features associated with the existence of Dirac Fermions have been predicted (Beenakker 2008). For example, due to the multiple conical valley band structure, the Andreev reflection, which usually is a retro-reflection (as seen in Figure 7.1), can be induced specularly with a high probability in undoped samples when the Fermi energy lies in the vicinity of the Dirac point (Beenakker 2006). Such effects, as well as the observation of peculiarities induced by the Andreev bound states (Titov and Beenakker 2006), require the realization of the ballistic graphene weak links, a challenging fabrication task since the mean free path of graphene samples usually made are below 0.1 μm. Promising routes are offered by making suspended graphene obtained by under-etching the supporting substrate. Such a process has been shown to greatly enhance the normal state electronic properties in the non-superconducting state by boosting mean free paths (Du et al. 2008b) and electronic mobilities (Bolotin et al. 2008).

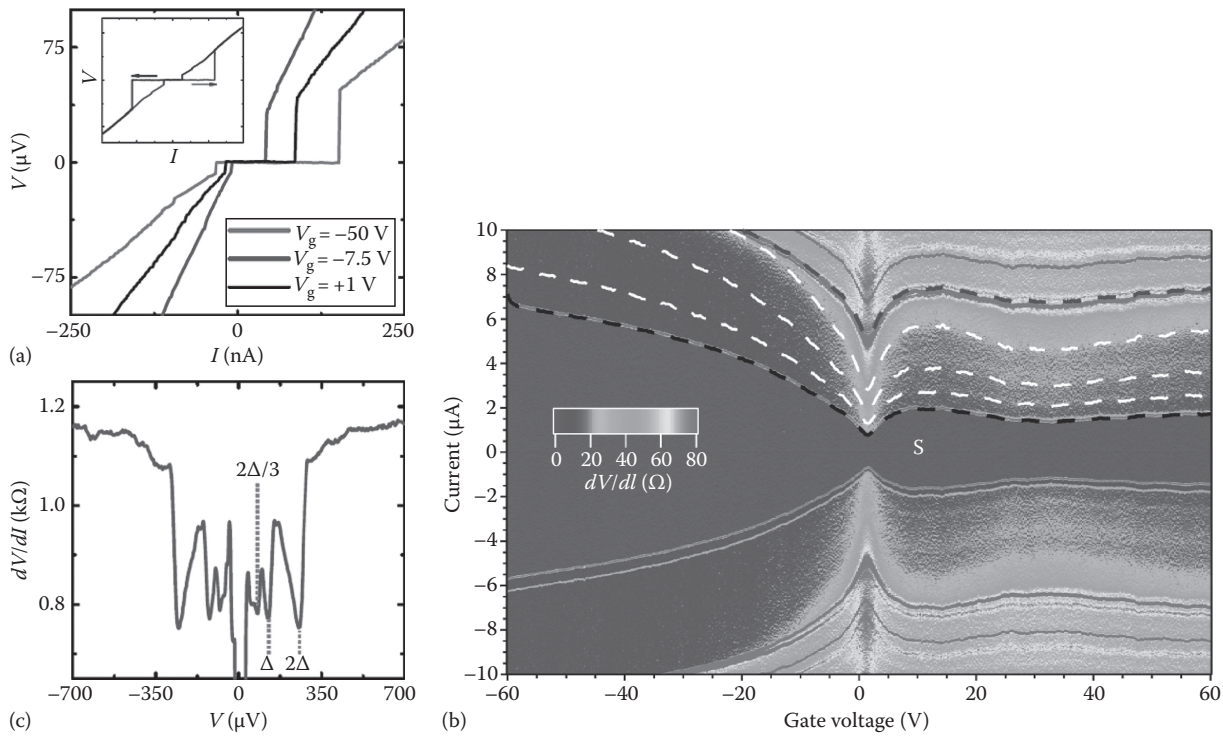

FIGURE 7.18 Characteristics of a superconducting/graphene/superconducting junction. (a) Voltage–current characteristics of a graphene-based superconducting weak link. (From Heersche, H.B. et al., *Nature*, 446, 56, 2007. With permission.) (b) Resistance map of a two-junction graphene device showing the ambipolar gate dependence of the superconducting state (central zone denoted by the letter S). Differential resistance of a device showing dependence of critical current on back gate voltage (yellow dashed line) at 20 mK. Traces of multiple Andreev reflections at constant voltages $2\Delta g/ne$ for $n = 1, 2, 3$ are indicated by the white dashed lines (n) 1 at top, $\Delta g \sim 75\,\mu$eV. (Adapted from Girit, Ç. et al., *Nano Lett.*, 9, 198, 2009.) (c) Differential resistance as a function of the voltage bias showing the multiple Andreev reflection peaks below the Gap 2D. (From Heersche, H.B. et al., *Nature*, 446, 56, 2007.)

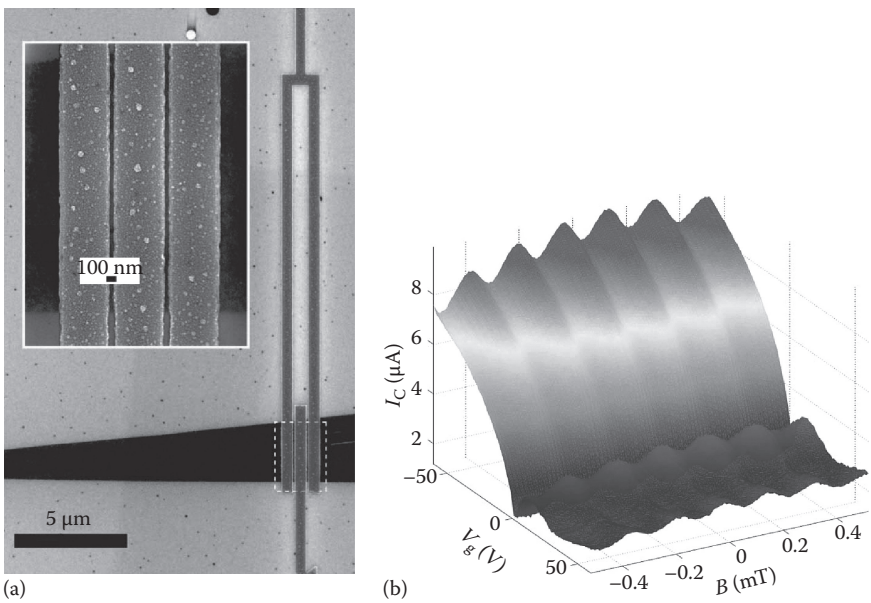

FIGURE 7.19 (a) Scanning electron microscope image of a superconducting quantum interference device with weak links made of portion of the same single layer graphene flake (black, graphene; gray, silicon oxide substrate; blue false-color, Pd/Al electrodes Inset: close-up of sub-100 nm wide graphene Josephson junctions. (b) Maximum switching current as a function of magnetic field B and gate voltage V_g. The sinusoidal oscillations indicate quantum interference between the two graphene Josephson junctions. For a fixed magnetic field, the magnitude of the modulation can be controlled by the back gate. (After Girit, Ç. et al., *Nano Lett.*, 9, 198, 2009.)

In the case of graphene, this is predicted to lead to an unusual bias dependence of the differential conductance of the weak link. In most experiments, superconducting charge carriers are injected by the measuring electrodes. However, it has been predicted (Feigel'man et al. 2010) and experimentally shown (Kessler et al. 2010) that the superconductivity could be induced globally by decorating the graphene with an array of superconducting electrodes. In this latter case, the proximity effect generates a supercurrent, which percolates through the entire graphene sheet.

7.5.2 Graphene Nanotube Superconducting Quantum Interferometers

Graphene-based SQUIDs devices can be obtained in a similar way as has been done for CNT weak links. Indeed, the fabrication and operation of a two junction SQUID formed by a single graphene sheet contacted with aluminum/palladium electrodes in the geometry of a loop (see Figure 7.19) has been demonstrated in 2009 (Girit et al. 2009).

As for the nanotube SQUID, graphene SQUIDs allow the tuning of the quantum interference with an electrostatic gate with a dependence (Figure 7.19b) that follows the transparency given by the graphene weak link (Figure 7.18). It also suggests a new modality for the ultrasensitive magnetometry of nanomagnets chemically or physically attached to the carbon surface.

7.6 Fullerene-Based Superconducting Weak Links

This last category considers the smallest sp^2 carbon weak links that involve fullerene molecules (Smalley 1997). We consider a device made of a fullerene molecule (see Figure 7.4a, right) placed in a transistor geometry (depicted in Figure 7.4b). Interaction of the discrete levels of a molecular entity with the superconducting electrode has triggered a lot a theoretical studies (Choi et al. 2004, Novotny et al. 2005). Unlike all the previous carbon-based weak links discussed above, for which the properties depend not only upon the material properties but also on the electrode geometries

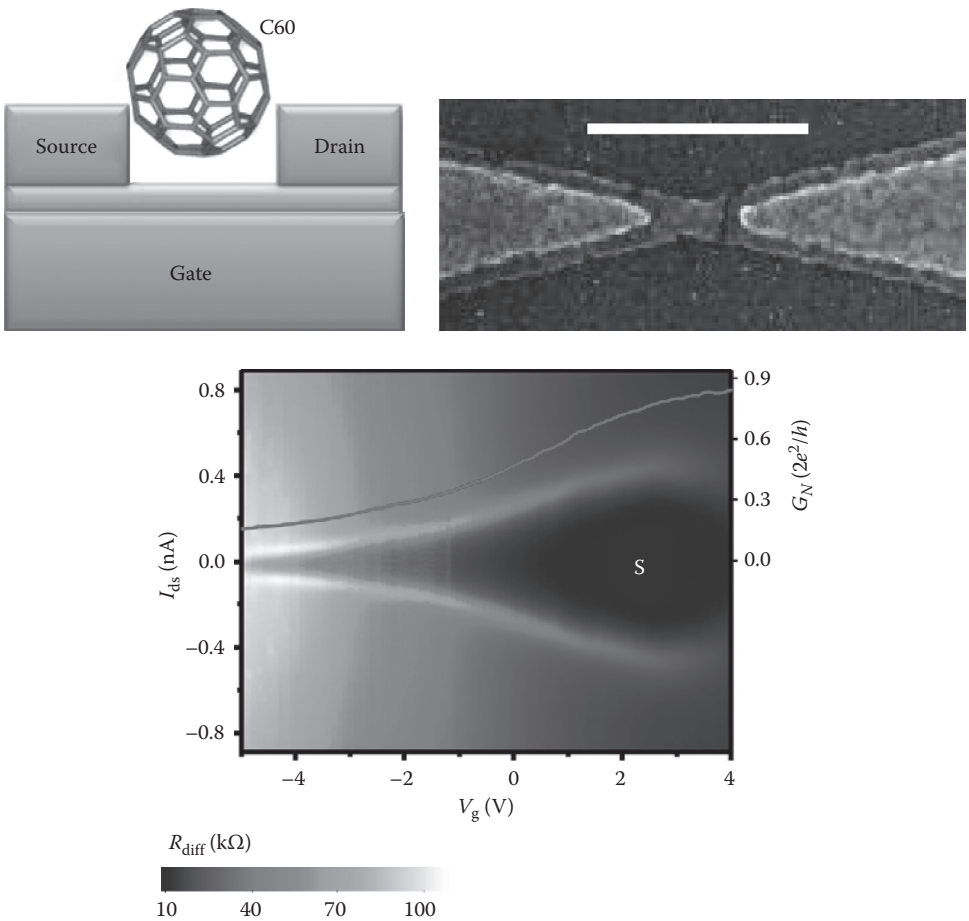

FIGURE 7.20 Fullerene based superconducting weak link. Top left: Schematics of the device C60 connected to superconducting source and drain. The device sits over an aluminum gate electrode whose thin native oxide forms the gate dielectrics. Top right: scanning electron micrograph of the device, showing the nanoscale gap created by electromigration. (scale bar = 300 nm). Bottom: Map of the differential resistance of the device as a function of the gate voltage (*x* axis) and the current bias (*y* axis). The black region corresponds to the superconducting state. The gate dependence of the superconducting current is in agreement with the expected dependence for a proximity coupled quantum dot. (After Winkelmann, C.B. et al., *Nat. Phys.*, 5, 876, 2009.)

(for example, in a nanotube weak link, we have seen that the weak link gate modulation is inversely proportional to the length of the weak link, which is defined by the gap between the electrode), fullerene-based weak links involve the entire molecule. Therefore, electron transport through the junction is supposed to exhibit fingerprints (Zazunov et al. 2006) linked to the intrinsic molecule states, such as vibrational modes (Park et al. 2000) or molecular magnetism (Lee et al. 2008). Indeed a set of experiments (see Figure 7.5, right) involving magnetically active molecules such as endofullerenes (Grose et al. 2008, Kasumov et al. 2005), which consist of additional atoms inserted in the carbon cage formed by the fullerene shell, are a sensitive probe of molecular magnetism.

7.6.1 Molecular Transistors Made by Electromigration

Recent progress in the field of molecular electronics now allows for the direct integration of molecular objects into electrical on-chip circuits. It has been shown that by inserting molecules into a nanometer gap by sectioning a metallic wire, it is possible to create a molecular transistor which conducting states are linked to molecular orbitals available for conduction (Park et al. 2000). This possibility was provided by the electromigration process (Park et al. 1999), which allows the generation of nanogaps in metallic wires with good yield and an unprecedented reproducibility.

7.6.2 Implementation of a C60 Superconducting Transistor

Such electromigration processes have been recently adapted to the fabrication of superconducting transistors involving a single C60 molecule inserted between gold/aluminum electrodes that can be measured at milliKelvin temperatures (Winkelmann et al. 2009). Figure 7.20 shows the gate control of the superconducting state achieved in this molecular transistor, in the case of low dissipation in the environment of the linking conductor. The observed switching current is significantly lower than the critical current and has been shown to follow the law

$$\frac{I_S}{I_0} = \left(1 - \sqrt{1 - \frac{G_N h}{2e^2}}\right)^{3/2}.$$

The results of a C60 molecular transistor (Winkelmann et al. 2009) show good agreement between the measured critical current as a function of gate voltage and the prediction for $I_c(V_g)$ when taking into account the phase oscillations across the weak link.

7.7 Concluding Remarks

A new class of molecular weak links has now become available for research, in which superconductors can be coupled with reliable transparent interfaces to nanostructures composed of a crystalline arrangement of sp^2-hybridized carbon. The main original feature offered by this new type of device is the tunability of the superconducting transport being possible through gate control of the weak link chemical potential offered by quantum confinement. The integration control over these nanostructures, which has been made possible by advances in nanofabrication, allows for the fabrication of hybrid devices that mix bottom-up and top-down approaches. They provide building blocks that pave the way for the realization of more complex devices that should be useful for quantum information and nanomagnetism.

Acknowledgment

The author warmly acknowledges Wolfgang Wernsdorfer for stimulating discussions.

References

Averin, D. and Bardas, A. 1995. ac Josephson effect in a single quantum channel. *Physical Review Letters*, 75: 1831.

Barone, A. and Paterno, G. 1982. *Physics and Applications of the Josephson Effect*. New York: John Wiley & Sons.

Beenakker, C. W. J. 2006. Specular Andreev reflection in graphene. *Physical Review Letters*, 97: 067007.

Beenakker, C. W. J. 2008. Colloquium: Andreev reflection and Klein tunneling in graphene. *Reviews of Modern Physics*, 80: 1337.

Beenakker, C. W. J. and van Houten, H. 1992. *Single-Electron Tunneling and Mesoscopic Devices* (eds. Koch, H. and Lübbig, H.) http://xxx.lanl.gov/abs/condmat/0111505l. Berlin, Germany: Springer.

Bena, C., Vishveshwara, S., Balents, L., and Fisher, M. P. A. 2002. Quantum entanglement in carbon nanotubes. *Physical Review Letters*, 89: 037901.

Bogani, L. and Wernsdorfer, W. 2008. Molecular spintronics using single-molecule magnets. *Nature Materials*, 7: 179.

Bogani, L., Danieli, C., Biavardi, E. et al. 2009. Single-molecule-magnet carbon-nanotube hybrids. *Angewandte Chemie*, 48: 746–750.

Bolotin, K. I., Sikes, K. J., Jiang, Z. et al. 2008. Ultrahigh electron mobility in suspended graphene. *Solid State Communications*, 146: 351.

Bouchiat, V. 2009. Detection of magnetic moments using a nano-SQUID: Limits of resolution and sensitivity in near-field SQUID magnetometry. *Superconductor Science and Technology*, 22: 064002.

Bouchiat, V., Chtchelkatchev, N., Feinberg, D. et al. 2003. Single-walled carbon nanotube–superconductor entangler: Noise correlations and Einstein–Podolsky–Rosen states. *Nanotechnology*, 14: 77–85.

Buitelaar, M. R., Nussbaumer, T., and Schonenberger, C. 2002. Quantum dot in the Kondo regime coupled to superconductors. *Physical Reviews Letters*, 89: 256801.

Burke, P. J. 2004. Ac performance of nanoelectronics: Towards a ballistic THz nanotube transistor. *Solid State Electronics*, 40: 1981.

Cao, J., Wang, Q., and Dai, H. 2005. Electron transport in very clean, as-grown suspended carbon nanotubes. *Nature Materials*, 4: 745–749.

Charlier, J.-C., Blase, X., and Roche, S. 2007. Electronic and transport properties of nanotubes. *Reviews of Modern Physics*, 79: 677.

Chen, R., Zhang, Y., Wang, D., and Dai, H. 2001. Non-covalent sidewall functionalization of single-walled carbon nanotubes for protein immobilization. *Journal of the American Chemical Society*, 123: 3838–3839.

Choi, M. S., Lee, M., Kang, K., and Belzig, W. 2004. Kondo effect and Josephson current through a quantum dot between two superconductors. *Physical Review B*, 70: 020502.

Clarke, J. and Braginski, A. I. 2004. *The SQUID Handbook*. Weinheim, Germany: Wiley-VCH.

Cleuziou, J.-P., Wernsdorfer, W., Bouchiat, V., Ondarcuhu, T., and Monthioux, M. 2006. Carbon nanotube superconducting quantum interference device. *Nature Nanotechnology*, 1: 53.

Cleuziou, J. P., Wernsdorfer, W., Andergassen, S. et al. 2007. Gate-tuned high frequency response of carbon nanotube Josephson junctions. *Physical Review Letters*, 99: 117001.

Courtois, H., Meschke, M., Peltonen, J. T., and Pekola, J. P. 2008. Origin of hysteresis in a proximity Josephson junction. *Physical Review Letters*, 101: 067002.

De Gennes, P. G. and Guyon, E. 1963. Superconductivity in "normal" metals. *Physics Letters*, 3: 168–169.

Du, X., Skachko, I., and Andrei, E. Y. 2008a. Josephson current and multiple Andreev reflections in graphene SNS junctions. *Physical Review B*, 77: 184507.

Du, X., Skachko, I., Barker, A., and Andrei, E. Y. 2008b. Approaching ballistic transport in suspended graphene. *Nature Nanotechnology*, 3: 491–495.

Feigel'man, M. V., Skvortsov, M. A., and Tikhonov, K. S. 2008. Proximity-induced superconductivity in graphene. *JETP Letters*, 88: 862.

Gang, L., Yong, Z., and Chun Ning, L. 2009. Gate-tunable dissipation and "superconductor-insulator" transition in carbon nanotube Josephson junctions. *Physical Review Letters*, 102: 016803.

Geim, A. K. and Novoselov, K. S. 2007. The rise of graphene. *Nature Materials*, 6: 183.

Girit, Ç., Bouchiat, V., Naaman, O. et al. 2009. Tunable graphene superconducting quantum interference device. *Nano Letters*, 9: 198–199.

Glazman, L. I. and Matveev, K. A. 1989. Resonant Josephson current through Kondo impurities in a tunnel barrier. *JETP Letters*, 49: 659.

Goffman, M. F., Cron, R., Levy Yeyati, A. et al. 2000. Supercurrent in atomic point contacts and Andreev states. *Physical Review Letters*, 85: 170.

Golubov, A. A., Kupriyanov, M. Y., and Il'ichev, E. 2004. The current-phase relation in Josephson junctions. *Reviews of Modern Physics*, 76: 411–469.

Grose, J. E., Tam, E. S., Timm, C. et al. 2008. Tunnelling spectra of individual magnetic endofullerene molecules. *Nature Materials*, 7: 884.

Hamilton, C. A. 2000. Josephson voltage standards. *Review of Scientific Instruments*, 71: 3611.

Heersche, H. B., Jarillo-Herrero, P., Oostinga, J. B., Vandersypen, L. M., and Morpurgo, A. F. 2007. Graphene JJ. *Nature*, 446: 56.

Herrmann, L. G., Portier, F., Roche, P. et al. 2010. Carbon nanotubes as cooper pair beam splitters. *Physical Review Letters*, 104: 026801.

Hofstetter, L., Csonka, S., Nygard, J., and Schonenberger, C. 2009. Cooper pair splitter realized in a two-quantum-dot Y-junction. *Nature*, 461: 960–963.

Imry, Y. and Landauer, R. 1999. Conductance viewed as transmission. *Reviews of Modern Physics*, 71: S306.

Jaklevic, R. C., Lambe, J., Silver, A. H., and Mercereau, J. E. 1964. Quantum interference effects in Josephson tunneling. *Physical Review Letters*, 12: 159–160.

Jarillo-Herrero, P., van Dam, J. A., and Kouwenhoven, L. P. 2006. Quantum supercurrent transistors in carbon nanotubes. *Nature*, 439: 953–956.

Javey, A., Guo, J., Wang, Q. et al. 2003. Ballistic carbon nanotube field-effect transistors. *Nature*, 424: 654–657.

Jørgensen, H. I., Grove-Rasmussen, K., Novotny, T., Flensberg, K., and Lindelof, P. E. 2006. Electron transport in single-wall carbon nanotube weak links in the Fabry-Perot regime. *Physical Review Letters*, 96: 207003.

Jorgensen, H. I., Novotny, T., Grove-Rasmussen, K., Flensberg, K., and Lindelof, P. E. 2007. Critical current 0-pi transition in designed Josephson quantum dot junctions. *Nano Letters*, 7: 2441–2445.

Josephson, B. D. 1962. Possible new effects in superconductive tunnelling. *Physics Letters*, 1: 251–253.

Kasumov, A. Y., Deblock, R., Kociak, M. et al. 1999. Supercurrents through single-walled carbon nanotubes. *Science*, 284: 1508.

Kasumov, A. Y., Tsukagoshi, K., Kawamura, M. et al. 2005. Proximity effect in a superconductor-metallofullerene-superconductor molecular junction. *Physical Review B*, 72: 033414.

Kessler, B. M., Girit, C. O., Zettl, A., and Bouchiat, V. 2010. Tunable superconducting phase transition in metal-decorated graphene sheets. *Physical Review Letters*, 104: 047001.

Klapwijk, T. M., Blonder, G. E., and Tinkham, M. 1982. Explanation of subharmonic energy gap structure in superconducting contacts. *Physica B*, 109: 1657.

Kouwenhoven, L. and Glazman, L. 2001. Revival of the Kondo Effect. *Physics World*, 14: 33.

Lassagne, B., Tarakanov, Y., Kinaret, J., Garcia-Sanchez, D., and Bachtold, A. 2009. Coupling mechanics to charge transport in carbon nanotube mechanical resonators. *Science*, 325: 1107–1110.

Lee, M., Jonckheere, T., and Martin, T. 2008. Josephson effect through a magnetic metallofullerene molecule. *Physical Review Letters*, 101: 146804.

Liang, W., Bockrath, M., Bozovic, D. et al. 2001. Fabry - Perot interference in a nanotube electron waveguide. *Nature*, 411: 665.

Likharev, K. K. 1979. Superconducting weak links. *Reviews of Modern Physics*, 51: 101.

Liu, G., Zhang, Y., and Lau, C. N. 2009. Gate-tunable dissipation and "Superconductor-insulator" transition in carbon nanotube Josephson junctions. *Physical Review Letters*, 102: 016803.

Morpurgo, A. F., Kong, J., Marcus, C. M., and Dai, H. 1999. Gate-controlled superconducting proximity effect in carbon nanotubes. *Science*, 286: 263–265.

Nemec, N., Tomanek, D., and Cuniberti, G. 2006. Contact dependence of carrier injection in carbon nanotubes: An Ab initio study. *Physical Review Letters*, 96: 076802.

Novotny, T., Rossini, A., and Flensberg, K. 2005. Josephson current through a molecular transistor in a dissipative environment. *Physical Review B*, 72: 224502.

Nygard, J., Cobden, D. H., and Lindelof, P. E. 2000. Kondo physics in carbon nanotubes. *Nature*, 408: 342–346.

Pallecchi, E., Gaaß, M., Ryndyk, D., and Strunk, C. 2008. Carbon nanotube Josephson junctions with Nb contacts. *Applied Physics Letters*, 93: 072501.

Park, H., Lim, A. K. L., Alivisatos, A. P., Park, J., and McEuen, P. L. 1999. Fabrication of metallic electrodes with nanometer separation by electromigration. *Applied Physics Letters*, 75: 301.

Park, H., Park, J., Lim, A. K. L. et al. 2000. Nanomechanical oscillations in a single-C60 transistor. *Nature*, 407: 57–60.

Recher, P. and Loss, D. 2002. Superconductor coupled to two Luttinger liquids as an entangler for electron spins. *Physical Review B*, 65: 165327.

Scheer, E., Joyez, P., Esteve, D., Urbina, C., and Devoret, M. H. 1997. Conduction channel transmissions of atomic-size aluminum contacts. *Physical Review Letters*, 78: 3535.

Smalley, R. E. 1997. Discovering the fullerenes. *Reviews of Modern Physics*, 69: 723.

Steele, G. A., Huttel, A. K., Witkamp, B. et al. 2009. Strong coupling between single-electron tunneling and nanomechanical motion. *Science*, 325: 1103–1107.

Titov, M. and Beenakker, C. W. J. 2006. Josephson effect in ballistic graphene. *Physical Review B*, 74: 041401.

Wernsdorfer, W. 2001. Classical and quantum magnetization reversal studies in nanometer-sized particles and clusters. *Advances in Chemical Physics*, 188: 99–190.

Wernsdorfer, W., Hasselbach, K., Mailly, D. et al. 1995. Seminal microSQUID particle WW. *Journal of Magnetism and Magnetic Materials*, 145: 33.

Wernsdorfer, W., Bonet Orozco, E., Hasselbach, K. et al. 1997. Macroscopic quantum tunneling of magnetization of single ferrimagnetic nanoparticles of Barium Ferrite. *Physical Review Letters*, 79: 4014–4017.

Winkelmann, C. B., Roch, N., Wernsdorfer, W., Bouchiat, V., and Balestro, F. 2009. Superconductivity in a single-C60 transistor. *Nature Physics*, 5: 876–879.

Zazunov, A., Fierberg, D., and Martin, T. 2006. Phonon squeezing in a superconducting molecular transistor. *Physical Review Letters*, 97: 196801.